Efficient CO2 Capture from Lime Plants: Techno-economic Assessment of Integrated Concepts using Indirectly Heated Carbonate Looping Technology

Publication Status:
Published online: 24/12/2023

DOI:
10.1016/j.ccst.2023.100187

Document Version
Version created as part of publication process; publisher's layout; not normally made publicly available

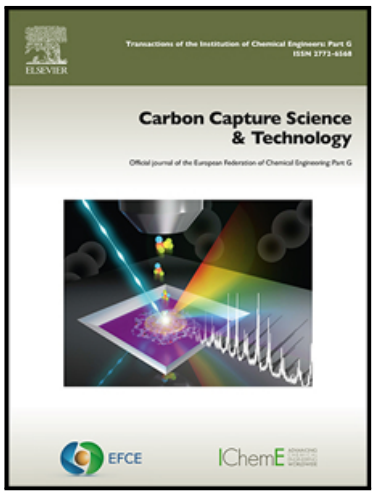

Efficient CO_2 Capture from Lime Plants: Techno-economic Assessment of Integrated Concepts using Indirectly Heated Carbonate Looping Technology

Martin Greco-Coppi , Peter Seufert , Carina Hofmann , Angela Rolfe , Ye Huang , Sina Rezvani , Jochen Ströhle , Bernd Epple

PII: S2772-6568(23)00091-X
DOI: https://doi.org/10.1016/j.ccst.2023.100187
Reference: CCST 100187

To appear in: *Carbon Capture Science & Technology*

Received date: 21 September 2023
Revised date: 8 December 2023
Accepted date: 24 December 2023

Please cite this article as: Martin Greco-Coppi , Peter Seufert , Carina Hofmann , Angela Rolfe , Ye Huang , Sina Rezvani , Jochen Ströhle , Bernd Epple , Efficient CO_2 Capture from Lime Plants: Techno-economic Assessment of Integrated Concepts using Indirectly Heated Carbonate Looping Technology, *Carbon Capture Science & Technology* (2023), doi: https://doi.org/10.1016/j.ccst.2023.100187

Highlights

- Techno-economic assessment on ten CO_2 capture configurations for lime production
- IHCaL technology is promising in terms of economic viability and energy efficiency
- Heat recovery strategies can be tailored to achieve different optimization outcomes
- CO_2 avoidance costs are low if solid recovered fuel (SRF) is used (less than 25 €/$t_{CO2,av}$)
- Computing negative CO_2 emissions further reduces the avoidance costs by around 25%

EFFICIENT CO_2 CAPTURE FROM LIME PLANTS: TECHNO-ECONOMIC ASSESSMENT OF INTEGRATED CONCEPTS USING INDIRECTLY HEATED CARBONATE LOOPING TECHNOLOGY

Martin Greco-Coppi[*,a], Peter Seufert[a], Carina Hofmann[a], Angela Rolfe[b], Ye Huang[b], Sina Rezvani[c], Jochen Ströhle[a], Bernd Epple[a]

[a]Institute for Energy Systems and Technology, Technical Univeristy of Darmstadt, Germany

[b]CST, Ulster University, United Kingdom

[c]ESTRA Energy Technology Strategies Ltd, United Kingdom

**Corresponding author. Corresponding author's e-mail address: martin.greco@est.tu-darmstadt.de*

ABSTRACT

The quest to decarbonize the lime and cement industry is challenging because of the amount and the nature of the CO_2 emissions. The process emissions from calcination are unavoidable unless carbon capture is deployed. Nevertheless, the majority of the available carbon capture technologies are expensive and energy inefficient. The indirectly heated carbonate looping (IHCaL) process is a promising technology to capture CO_2 from the lime and cement production, featuring low penalties in terms of economics and energy utilization. Previous works have highlighted the potential of the IHCaL, but the optimization of the process has not been discussed in enough detail and techno-economic implications are not yet fully understood. Within this work, ten scenarios using IHCaL technology to capture CO_2 from a lime plant were simulated. Hereby, different process configurations, heat recovery strategies and fueling options were computed. The calculations for the capture facilities were performed with Aspen Plus® software and EBSILON®*Professional* was used to simulate the steam cycles. A techno-economic assessment was included as well, aided by the ECLIPSE software.

The results demonstrate that the selection of the fuel for the combustor not only affects the CO_2 balance and energy performance but is also an important cost driver —there were considerable economic advantages for the computed cases with middle-caloric solid recovered fuel (SRF). The analysis shows how the heat recovery strategy can be optimized to achieve tailored outcomes, such as reduced fuel requirement or increased power production. The specific primary energy consumption (from –0.3 to +2.5 $MJ_{LHV}/t_{CO2,av}$) and cost for CO_2 avoided (from –11 to +25 €/$t_{CO2,av}$) using SRF are considerably low, compared with other technologies for the same application. The sensitivity study revealed that the main parameters that impact the economics are the discount rate and the project life. The capture plants are more sensitive to parameter changes than the reference plant, and the plants using SRF are more sensitive than the lignite-fueled plants. The conclusions from this work open a new pathway of experimental research to

validate key assumptions and enable the industrial deployment of IHCaL technology before 2030.

Keywords: indirectly heated carbonate looping; techno-economic assessment; solid recovered fuel (SRF); CO_2 capture in the lime production; heat recovery optimization; carbon dioxide removal (CDR)

LATIN SYMBOLS

BESP	(€/t_{lime})	Breakeven selling price
e_{CO2}	(g_{CO2}/kg_{CaO})	Specific CO_2 emission
$e_{ref,el}$	(g_{CO2}/ MJ)	CO_2 emissions factor of the grid
$e_{CO2,fuel}$	(g_{CO2}/MJ_{LHV})	Fuel specific CO_2 emissions
E_{cc}	(–)	Carbon capture efficiency
f_m; f_w	(–)	Fitting constants for Eq.(3)
F_{CO2}	(mol_{CO2}/s)	CO_2 molar flow rate (into carbonator)
F_t	(M€)	Fuel expenditure in year *t*
F_R	(mol_{Ca}/s)	Sorbent molar circulation rate
F_0	(mol_{CaCO3}/s)	Make-up molar flow rate
HtPR	(–)	Heat-to-power ratio
HR	(–)	Specific heat ratio
HR_a	(–)	Absolute heat ratio
I_t	(M€)	Investment expenditure (CAPEX) in year *t*
I_0	(M€)	Initial investment expenditure (initial CAPEX)
LHV	(kJ/kg)	Lower heating value
$\dot{m}_{CaO}$	(t/h)	Product mass flow rate
$\dot{m}_{fuel}$	(t/h)	Fuel mass flow rate/ fuel requirement
$\dot{m}_{CO2}$	(t/h)	CO_2 mass flow rate
M_t	(M€)	Operation and maintenance expenditure in year *t*
n	(year)	System lifetime
p	(bar)	Pressure
P_{el}	(MW)	Electric power
PR	(–)	Product ratio

q	(J/kg_{CaO})	Specific primary energy consumption
$\dot{Q}$	(MW)	Heat flow rate/ heat duty
r	(%)	Discount rate
$SPECCA$	($MJ_{LHV}/kg_{CO2,av}$)	Specific primary energy consumption for CO_2 avoided
T	(°C)	Temperature
u_0	(m/s)	Free gas velocity
x_{bio}	(–)	Fuel carbon biogenic fraction
X	(mol_{CaCO3}/mol_{Ca})	Degree of carbonation
$X_{ave,max}$	(mol_{CaCO3}/mol_{Ca})	Maximum carbonation after carbonator (sorbent activity)

GREEK SYMBOLS

Δp	(mbar)	Pressure drop through component/reactor
$\eta_{net,SC}$	(–)	Steam cycle net efficiency
$\eta_{ref,el}$	(–)	Reference electrical efficiency of the grid
Λ	(mol_{CaCO3}/mol_{CO2})	Specific make-up rate
Φ	(mol_{Ca}/mol_{CO2})	Specific sorbent circulation rate

ABREVIATIONS

ASU	Air separation unit
BECCS	Bioenergy with carbon capture and storage
bio	Biogenic (fraction)
CaL	Carbonate looping/ Calcium looping
CAPEX	Capital expenditure
CEPCI	Chemical Engineering Plant Cost Index
CCS	Carbon capture and storage
CDR	CO_2 removal
ECO	Economizer
EPC	Engineering, procurement and construction (cost)
ES	Energy scenario
EU-28	European Union (energy mix)
EVA	Evaporator

IHCaL	Indirectly heated carbonate looping
KPI	Key performance indicator
Leilac	Low emissions intensity lime and cement (project)
MEA	Monoethanolamine
NGCC	Natural gas combined cycle
NPV	Net present value
OPEX	Operating expenditure
O&M	Operating and maintenance (costs)
PRK	Preheated rotary kiln (reference/host facility)
RDF	Refuse-derived fuel
RH	Reheater
ROI	Return on investment
S	Process scenario
SH	Superheater
SRF	Solid recovered fuel
TEA	Techno-economic assessment
TCC	Total capital cost

SUBSCRIPTS AND SUPERSCRIPTS

bio	Biogenic fraction
calc	calciner/calciner exit
capt	captured CO_2
carb	carbonator/ carbonator exit
comb	combustor/ combustor exit
foss	Fossil fraction
FA	Fluidization agent
FG	Flue gas
ref	Reference facility without carbon capture
SC	Steam cycle
wet	Wet basis

1. INTRODUCTION

The production of lime and cement is responsible for around 8% of global anthropogenic CO_2 emissions (Andrew, 2018). About 65% of these emissions are associated with the calcination of limestone (IEA, 2020; Schorcht et al., 2013) and can only be avoided with carbon capture. There are many carbon capture technologies available —absorption, e.g., using methanolamine (MEA); adsorption; membrane separation; cryogenic capture; oxy-fuel combustion; chemical and carbonate looping; and biological CO_2 removal—, but the majority have high thermodynamic and economic penalties (Da Cachola et al., 2023; Hong, 2022; Krishnan et al., 2023; Voldsund et al., 2019).

One promising technology that may be used to decarbonize the lime industry is the direct separation of the Leilac-1 —low emissions intensity lime and cement— project (Hills et al., 2017), which uses an indirectly heated vertical tube for the calcination. Direct separation enables capture for all the process emissions with low cost (Driver et al., 2022), but is not able to separate the CO_2 produced by combustion. This technology has been demonstrated up to the 240 t/d raw meal scale, separating 85 t/d of CO_2. A scale-up of the technology will take place within the Leilac-2 project (European Commission, 2020). The start of construction is scheduled for the year 2023.

Among the available technologies for capturing CO_2 from lime and cement production, carbonate looping (CaL) (Shimizu et al., 1999) is one of the most promising, because it can enable synergies with the calcination process, and thus allow to capture CO_2 efficiently without incurring high costs (De Lena et al., 2022; Zhao et al., 2013). The CaL process (see Figure 1) operates with two reactors, namely, a carbonator (ca. 650 °C) and a calciner (ca. 900 °C), using solid sorbents, such as lime (mainly CaO). The high temperatures enable manifold regenerative heat integration options. The operating principle is the reversible carbonation-calcination reaction of CaO. CO_2 from flue gases is bound through carbonation of the sorbent inside the carbonator, which typically operates in the bubbling or circulating fluidized bed regime (Abanades et al., 2004; Charitos et al., 2011). The carbonated sorbent is regenerated in the calciner, also operating as a fluidized bed reactor (Wang et al., 2007). In the standard configuration, the heat for the calcination is provided via oxy-fuel combustion, directly in the combustor, using pure oxygen and fuel (see Myöhänen et al., 2009). CaL technology has been demonstrated up to the pilot scale for manifold operating conditions (Arias et al., 2017; Arias et al., 2013; Diego et al., 2016b; Dieter et al., 2014; Kremer et al., 2013; Ströhle et al., 2014), including firing with waste-derived fuels (Haaf et al., 2020c; Haaf et al., 2020b).

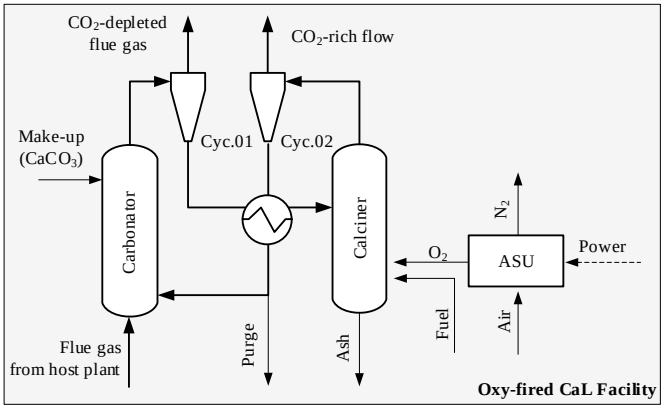

Figure 1. Oxy-fired carbonate looping process with air separation unit (ASU).

The drawback of standard CaL technology is the requirement of pure oxygen, which is obtained with an energy-intensive air separation unit (ASU). The installation of an ASU entails significant investment. De Lena et al. (2022) calculated that the ASU accounts for around 15% of the total plant cost for an integrated CaL system for CO_2 capture from a cement plant. A similar result was obtained by Fu et al. (2021) for the implementation of the CaL process in natural gas combined cycle plants. Additionally, the electric power required to operate the ASU can be higher than 40% of the electricity demand of the entire CaL system (De Lena et al., 2022; Haaf et al., 2020a).

From the entire carbon capture and storage (CCS) value chain —separation, transport, and geological storage—, the capture process is the most energetically demanding and it accounts for about 70–80% of the total costs (Vitillo et al., 2017). Santos and Hanak (2022) reviewed the available techno-economic analysis studies on carbon capture for industrial processes of the last ten years. They concluded CaL is superior to other technologies (amine scrubbing, physical absorption, vacuum pressure swing absorption, and oxy-fuel combustion) for this kind of application. According to their estimations, CaL technology has an average CO_2 avoidance cost of 32.7 to 42.9 €/$t_{CO2,av}$ and an equivalent energy requirement between 2.0 and 3.7 $MJ_{th}/kg_{CO2,av.}$ Membrane separation technology —which was not included in the review of Santos and Hanak (2022)— is sometimes regarded as a competitive alternative to decarbonize the cement industry, but it is still costly (> 80 EUR/$t_{CO2,av}$) if capture rates of more than 80 % are to be achieved (Baker et al., 2018; Ferrari et al., 2021; Gardarsdottir et al., 2019). De Lena et al. (2019) analyzed carbonate looping technology for cement plants and obtained slightly higher costs (52 €/$t_{CO2,av}$ – 58.5 €/$t_{CO2,av}$) for the scenarios considered. Romano et al. (2013) presented an integrated concept for cement production and power generation that would be profitable even for low carbon taxes, starting at 27 €/t_{CO2}.

Gardarsdottir et al. (2019) compared different carbon capture technologies for the cement production. According to their calculations, the lowest avoidance costs, amounting to 42 €/$t_{CO2,av}$, would be achieved with oxy-fuel technology. However, they explained that retrofitability issues might negatively impact the cost performance of the oxy-fuel process. Cormos et al. (2020) evaluated capture technologies to decarbonize different industrial processes, including cement production, for which they estimated that a 90% decarbonization rate could be achieved with a cost of 57.8 €/$t_{CO2,av}$ with CaL technology. Yang et al. (2021) carried out an extensive techno-

economic analysis, in which they considered numerous carbon capture technologies and integration options. One of their most relevant findings is that the utilization of biomass with carbon capture and storage, i.e., BECCS, improves the technical and economic performance of the CO_2 capture. To date, not many works have been published analyzing the costs of capturing CO_2 from lime plants. Moreover, there are many similarities between lime and cement production; therefore, conclusions about CO_2 capture can be extrapolated from one industry to the other —see Greco-Coppi et al. (2023) for a throughout discussion on this matter.

To reduce the penalties of the CaL, the heat for the calcination can be provided indirectly, thus eliminating the need for an ASU. This technology is known as the indirectly heated carbonate looping (IHCaL) (Junk et al., 2013). Indirect heating can be achieved with different mechanisms, such as utilization of steam (Fan, 2012; Ramkumar and Fan, 2010; Wang et al., 2010), direct heat transfer through the reactor walls (Abanades et al., 2005; Grasa and Abanades, 2007), or by means of solid heat carriers (Abanades et al., 2005; Diego et al., 2016a; Martínez et al., 2011). One of the most promising approaches consists of utilizing heat pipes connecting the calciner and the combustor (Hoeftberger and Karl, 2016; Junk et al., 2013; Reitz et al., 2014). The IHCaL technology utilizing heat-pipes to indirectly heat the calciner has been validated during pilot testing at the 300 kW_{th} scale test rig of the Technical University of Darmstadt (Reitz et al., 2016), including operation in relevant conditions for the lime industry (Hofmann et al., 2024, 2022a). Junk et al. (2016) estimated that the CO_2 avoidance cost for a coal power plant with IHCaL technology would be 22.6 €/$t_{CO2,av}$.

Greco-Coppi et al. (2021) developed the IHCaL process for use in lime plants and indicated the importance of heat recovery in the global process efficiency, due to the high temperatures of the process (over 650 °C). They presented two possible configurations to produce lime with low CO_2 emissions: (i) a tail-end configuration, which is useful for retrofitting an existing lime kiln (see Figure 2); and (ii) a fully integrated solution (see Figure 3).

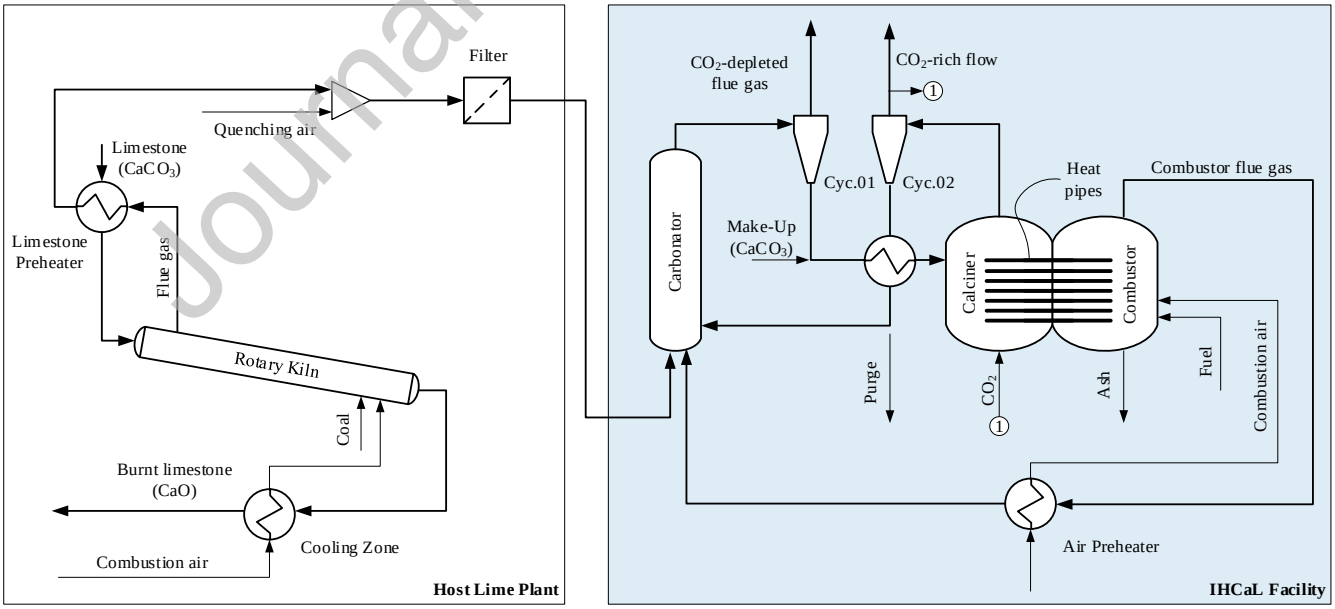

Figure 2. Lime production facility with carbon capture using a retrofitted indirectly heated carbonate looping process (IHCaL), adapted from Greco-Coppi et al. (2021) with permission of Elsevier.

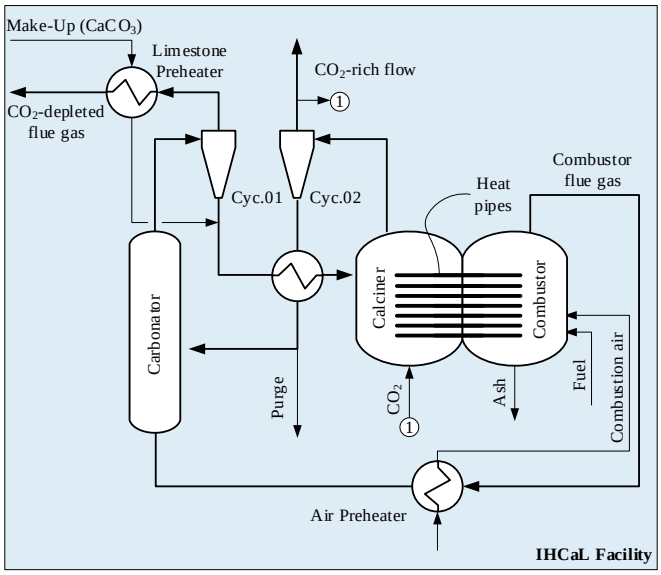

Figure 3. Lime production facility with carbon capture using a fully integrated IHCaL facility to produce lime with low CO2 emissions, adapted from Greco-Coppi et al. (2021) with permission of Elsevier.

The tail-end configuration consists in an IHCaL facility placed downstream of a host lime plant, as shown in Figure 2. It permits capturing CO_2 with minimal impact on the upstream process. Additionally, it expands the production capacity of the entire facility through the utilization of spent sorbent (purge stream).

The fully integrated solution (illustrated in Figure 3) involves the construction of a completely new facility; thus, it is not suitable for retrofitting existing lime kilns. This new facility constitutes an entire lime production plant with integrated carbon capture through carbonate looping, where the make-up stream is the raw limestone and the purge stream is the product (lime). A detailed explanation of the two configuration concepts can be found in previous publications (Greco-Coppi et al., 2023; Greco-Coppi et al., 2021; Junk et al., 2013).

A detailed analysis and optimization of the heat recovery system —indispensable to exploit the potential of the IHCaL in the lime production— is yet to be done. Furthermore, the advantage of utilizing waste-derived fuel —such as solid recovered fuel (SRF) or refuse-derived fuel (RDF) (see Gerassimidou et al., 2020; Sarc and Lorber, 2013; Velis et al., 2010)— to produce the heat for the combustion was established (Greco-Coppi et al., 2023), but the techno-economic impact is not fully understood yet.

This work closes an important knowledge gap in the route to develop the IHCaL process by delineating the economic and technical implications of applying this technology to the lime production. To achieve this, a comprehensive process modeling of the IHCaL process is performed. Furthermore, the design of the heat recovery steam cycle is investigated and three alternative heat recovery strategies are analyzed. For the heat production in the combustor, two options are evaluated, namely, utilizing lignite or fueling SRF. Altogether, eleven process scenarios are compared with each other in terms of CO_2 formation, energy utilization, and economic performance. Finally, a sensitivity analysis is included.

2. METHODS

2.1. IHCaL Process and Scenarios Analyzed

In this work, different strategies to reduce CO_2 emissions in the lime production were analyzed. An operating lime production plant from Germany was taken as the reference facility for the study and the host plant for the retrofitting configurations. This plant utilizes a preheated rotary kiln (PRK) for the calcination of limestone. It is described in detail in the work of Greco-Coppi et al. (2021).

The different process scenarios (S) that were studied differ in terms of plant concept, fuel type for the combustor, and heat recovery concept (see section 2.2 for this last category). In total, eleven scenarios were computed (see Table 1): the reference German lime plant as-built, without carbon capture (S-1); four retrofitting or "tail-end" configurations for lime production with carbon capture using lignite (S-2 and S-3) and SRF (S-4 and S-5); as well as six fully integrated solutions using lignite (S-6 to S-8) and SRF (S-9 to S-11).

Table 1. Process scenarios calculated

Plant concept	**IHCaL integration**	**Fuel IHCaL combustor**	**Heat recovery concept***	**Scenario number**
Reference PRK	N/A	N/A	N/A	S-1
PRK with downstream carbon capture (see Figure 2)	Tail-end	Lignite	I	S-2
			II	S-3
		SRF	I	S-4
			II	S-5
Lime production facility with fully integrated carbon capture (see Figure 3)	Fully integrated	Lignite	I	S-6
			II	S-7
			III	S-8
		SRF	I	S-9
			II	S-10
			III	S-11

*I: only air preheater; II: heat exchanger before air preheater; III: heat exchanger after air preheater

Greco-Coppi et al. (2023) showed that fueling the IHCaL with waste-derived fuels allows for carbon dioxide removal (CDR) through negative CO_2 emissions (Kemper, 2015; Yang et al., 2021). This holds true if the biogenic fraction (bio) of CO_2 from the combustion is captured and effectively removed from the atmosphere —mainly through subsequent geological storage.

The fuels for this analysis were selected following the work from Greco-Coppi et al. (2023). The lignite properties were obtained from the fuel analysis of the lignite used in the host plant in Germany. The properties of the SRF implemented in this work are consistent with the SRF used to successfully operate the 1 MW_{th} CaL plant in Darmstadt (Haaf et al., 2020d; Haaf et al., 2020b). The composition and main properties of the fuels are presented in Table 2, where *LHV* is the lower heating value in wet basis, x_{bio} is the carbon biogenic fraction in the fuel (Astrup et al., 2009; Moora et al., 2017), and $e_{CO2,fuel}$ is the fuel CO_2 emissions index (Furimsky, 2007; Madejski et al., 2022), i.e., the specific CO_2 emissions for the combustion of the fuel.

Table 2. Input data of the fuels, adopted from Greco-Coppi et al. (2023).

Parameter	Unit	Dried lignite	SRF
LHV	MJ/kg_{wet}	21.5	15.7
x_{bio}	%	0	45
$e_{CO2,fuel}$	g_{CO2}/MJ_{LHV}	96.7	88.7
Particle size	mm	0 – 4	$d_{95} < 50$
C	$wt.\%_{wet}$	56.7	38.0
H	$wt.\%_{wet}$	4.3	5.2
N	$wt.\%_{wet}$	0.7	1.0
S	$wt.\%_{wet}$	0.8	0.3
O	$wt.\%_{wet}$	21.5	19.9
Cl	$wt.\%_{wet}$	0.2	0.7
H_2O	$wt.\%_{wet}$	10.3	19.4
Ash	$wt.\%_{wet}$	5.5	15.4
Reference		Greco-Coppi et al. (2021)	Haaf et al. (2020d)

Figure 4 is a simplified IHCaL flow diagram that shows the main molar flows (F) of sorbent and CO_2, as well as the sorbent carbonation degrees (X). The sorbent molar flow rates are F_R, for the sorbent circulation between the carbonator and calciner, and F_0, for the fresh make-up and the purge streams. The make-up stream consists of pure limestone (mainly $CaCO_3$). The total CO_2 molar flow rate into the carbonator is indicated with F_{CO2}.

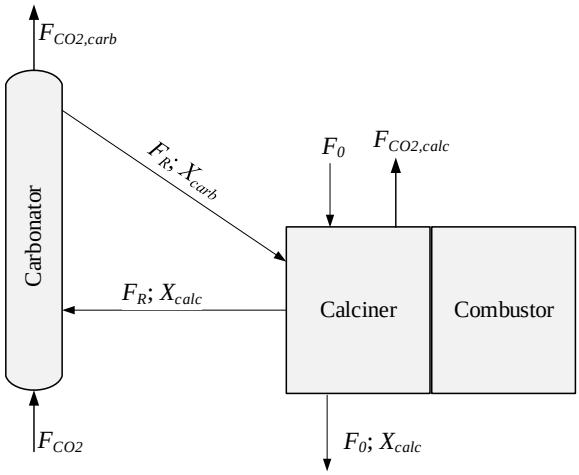

Figure 4. Indirectly heated carbonate looping process: simple process diagram with main molar flow and carbonization degrees parameters.

For the calculations and the comparisons, it is generally useful to work with dimensionless parameters; thus, the specific make-up rate (Λ) and the specific sorbent circulation rate (Φ) are defined according to Eq.(1) and Eq.(2), respectively. These parameters are varied in order to optimize the processes (Greco-Coppi et al., 2021).

$$\Lambda = \frac{F_0}{F_{CO2}} \tag{1}$$

$$\Phi = \frac{F_R}{F_{CO2}} \tag{2}$$

2.2. Heat Recovery and Steam Cycle

Due to the high operating temperatures (>650°C), the IHCaL process offers the possibility of recovering heat by means of a steam cycle. The usable sources for heat recovery are:

- CO_2-depleted flue gas from the carbonator (650°C)
- CO_2-rich flow from the calciner (900°C)
- Flue gases from the combustor (1000°C)
- Heat from the carbonator cooling (650°C)

The flue gas from the external combustion chamber has a temperature of 1000°C. This stream is used to preheat the combustion air (see Figure 2 and Figure 3). It is necessary to investigate how the use of the flue gas for steam generation affects the preheating temperature, which in turn has an important impact in the fuel requirement for the carbon capture (cf. Greco-Coppi et al., 2021).

Another point of integration is the utilization of the carbonator flue gases to preheat the fresh limestone before it enters the system, prior to exchanging heat with the steam cycle (see Figure 3). It is included for all the fully integrated concepts (S-6 to S-11). This heat recovery strategy is not implemented in the tail-end configurations (S-2 to S-5), where the specific make-up rates are much lower and the energy penalty of heating the make-up is negligible.

Considering the impact of the heat recovery on the energy balance, three recovery concepts were developed (illustrated in Figure 5). The proposed concepts are analyzed and discussed to understand the effect of the heat recovery in the IHCaL process.

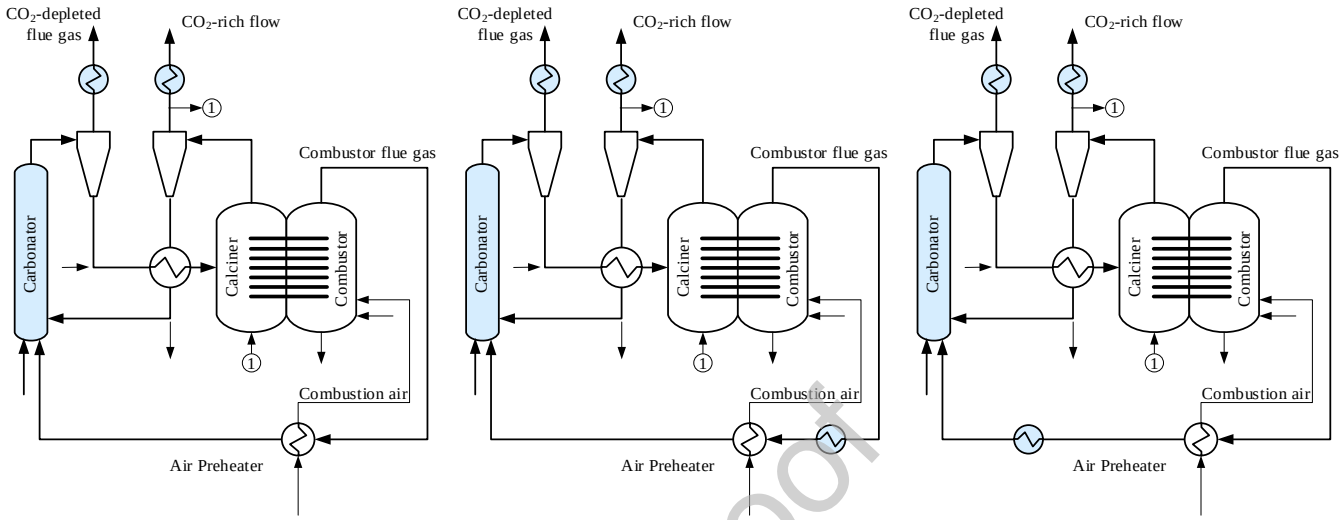

Figure 5. Concepts for the recovery of heat from the IHCaL facility. The configurations differ in the utilization of the heat from the combustor flue gases: (a) only for air preheating (concept I), (b) in the steam cycle before the air preheater (concept II), and (c) in the steam cycle after the air preheating (concept III). The heat exchangers used to transfer heat to the steam cycle are indicated with a blue shading.

In configuration (I) (Figure 5.a), the flue gas is not used to transfer heat into the steam cycle, but only for the preheating of the combustor air. Thus, the IHCaL process is not affected by the heat recovery. This approach has the advantage that the complexity of the steam cycle is significantly reduced. An air preheating temperature of 800°C can be achieved so that fuel consumption is kept as low as possible. However, this approach has the consequence that less power is generated within the steam cycle, so that some optimizations (e.g., reheating) are no longer economical.

The second approach (II) (Figure 5.b) consists in recovering heat from the flue gas directly downstream of the combustion chamber. Thus, the flue gas is cooled before using it for air preheating. The advantage of this approach is that significantly more heat is available for the steam cycle; thus, higher power output can be achieved, which means that further optimization of the steam cycle is worth implementing. The subsequent air preheating with the flue gas heats the air to approx. 450-500°C. These preheating temperatures are achievable with the current state-of-the-art air preheaters. The disadvantage of configuration (II) is that the preheating temperature of the combustion air is significantly lower than in the reference case (≈ 40% lower). This leads to a higher fuel requirement to provide the necessary heat for the calciner.

To compensate for the disadvantages of configurations (I) and (II), a third concept (III) was considered (Figure 5.c). It is analogous to approach (II), but in this case, the flue gas is used for steam generation after air preheating; thus, less energy is lost, which increases the overall energy efficiency of the system.

Energy involved in the compression of CO_2 could be partially recovered, e.g., through feed-water preheating. Hanak et al. (2014) evaluated different options to optimize the electric generation of a coal-fired steam power plant retrofitted with an integrated CO_2 capture process. He concluded that utilizing the intercooler heat for the feed-water heating is not as efficient in

terms of cost, compared to, e.g., using flue gas for this purpose. Consequently, it was decided to leave the heat recovery from the CO_2 compression train out of this analysis.

The three concepts for recovery (I, II, and III) were studied for the tail-end and the fully integrated IHCaL processes utilizing lignite and SRF to fuel the combustor (see Table 1). Since the temperature of the flue gas after the air preheater was too low to justify the addition of a heat exchanger in the tail-end configuration, concept (III) in the tail-end integration was deemed unrealistic and was not pursued; thus, the results of the tail-end concept are only presented for heat recovery concepts (I) and (II). The detailed investigation of the variation of the steam cycle with the fuel was out of the scope of this work. For the calculations of the steam cycle, the results from the simulations with lignite were used. The cycle's efficiency was assumed invariant with the fuel used in the IHCaL, and the heat recovered was scaled-up with the heat input in the IHCaL process. This assumption is reasonable considering the similar CO_2 emission factor ($e_{CO2,fuel}$) of the fuels in this work, and the low variation of firing capacity with the fuels considered (see Section 3.1). Furthermore, the results of the simulations show a very small variation of heat requirement in the calciner with the fuel type (less than 3% for all cases), which further supports the assumption. A special discussion on chloride-assisted corrosion is included in Section 3.1, since many waste-derived fuels have high chlorine content.

The main assumptions for the design of the steam cycles are presented in Table 3. To increase the efficiency of the steam cycle, regenerative feed-water preheating from turbine extractions was considered (Böckh and Stripf, 2018). Menny (2006) recommended 6 to 10 extractions for commercial facilities. In this work, 6 extractions were assumed considering the relatively low power output of the process, except for the fully integrated scenario (II), for which 5 extractions were considered, due to the lower power output (< 10 MW_{el}). The isentropic efficiency of the turbines was specified using data from Consonni and Viganò (2012), together with preliminary estimations of heat recovery. The configuration of the heat exchangers is presented in Table 3, in the sequence order viewed from the process side. The numbering of the heat exchangers corresponds to the sequence viewed form the steam side. For parallel heat exchangers, the same numbering is used.

A flow diagram of one steam cycle is included in Figure 6 for illustration purposes. It corresponds to the fully integrated heat recovery configuration with upstream combustion air preheating (recovery concept III). Heat is recovered from the carbonator cooling system in the evaporator (EVA) and superheater (SH 1), from the CO_2-depleated flue gas exiting the carbonator in the economizer (ECO 2), from the combustor flue gas in the superheater (SH 2), and from the high purity CO_2 stream leaving the calciner in the superheater (SH 3) and the economizer (ECO 1).The fresh limestone ($CaCO_3$-PH) and the combustion air (Air-PH) are preheated with the flue gases from the carbonator and the combustor, respectively. The feed-water preheating is not included in the illustration for simplicity.

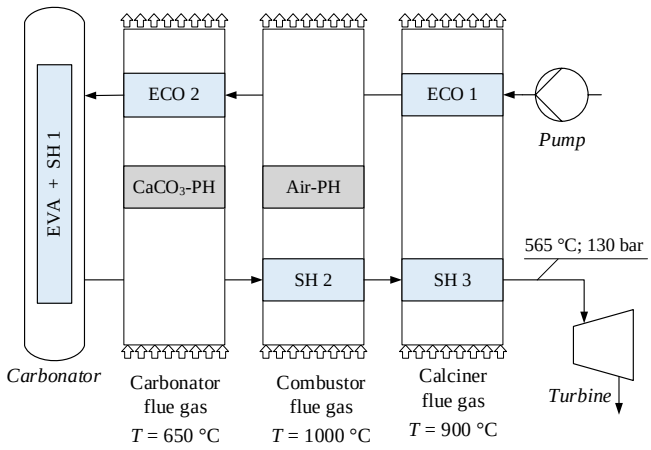

Figure 6. Flow diagram of one steam cycle to recover heat from the IHCaL-facility, corresponding to the fully integrated (III) scenario. In this configuration, heat is recovered from the carbonator cooling system in the evaporator (EVA) and superheater (SH 1), from the CO_2-depleated flue gas exiting the carbonator in the economizer (ECO 2), from the combustor flue gas in the superheater (SH 2), and from the high purity CO_2 stream leaving the calciner in the superheater (SH 3) and the economizer (ECO 1). The fresh limestone ($CaCO_3$-PH) and the combustion air (Air-PH) are preheated with the flue gases from the carbonator and the combustor, respectively.

Table 3. Main assumptions for the steam cycles

Configuration	**Tail-end**		**Fully integrated**		
Heat recovery concept	**I**	**II**	**I**	**II**	**III**
Turbine efficiency					
Mechanical	99.5%	99.5%	99.5%	99.5%	99.5%
Isentropic	85%	85%	82%	82%	82%
Generator efficiency	98.6%	98.6%	98.6%	98.6%	98.6%
Pump efficiency					
Mechanical	99.8%	99.8%	99.8%	99.8%	99.8%
Isentropic	80%	80%	80%	80%	80%
Superheater					
p (bar)	130	130	130	130	130
T (°C)	565	565	565	565	565
Reheater					
p (bar)	–	30	–	–	–
T (°C)	–	565	–	–	–
Exhaust					
p (bar)	0.07	0.07	0.07	0.07	0.07
Feed-water preheating	6	6	5	6	6
Carbonator					
Heat exchangers	EVA; SH1	EVA	EVA; SH1	EVA	EVA; SH1
Carbonator flue gas					
Heat exchangers	SH2; ECO	SH1; EVA; ECO	ECO	ECO	ECO2
T_{in} (°C)	650	650	420	430	430
T_{out} (°C)	286	266	276	266	266
Calciner flue gas					
Heat exchangers	SH3; ECO	SH2; ECO	SH2; ECO	EVA	SH3; ECO1
T_{in} (°C)	900	900	900	900	900
T_{out} (°C)	286	266	276	344	503
Combustor flue gas					
Heat exchangers	–	RH; SH3	–	SH	SH2
T_{in} (°C)	–	1000	–	1000	600
T_{out} (°C)	–	604	–	737	450

EVA: Evaporator; ECO: Economizer; SH: Superheater; RH: Reheater

2.3. Process Modeling

For the calculation of heat and mass balances, and the main thermodynamic key performance indicators (KPIs), process simulation software was utilized. The lime plant and IHCaL facilities were calculated with the software Aspen Plus® (Aspen Technology, Inc., 2020). The steam cycle was simulated and optimized with the aid of EBSILON®*Professional* software (Steag Energy Services GmbH, 2022). The input data for the steam cycle model was taken from the Aspen Plus® simulations.

The Aspen Plus® simulations were performed using available material property data (ASPEN APV120 database) and property methods (Aspen Technology, Inc., 2001). The Redlich-Kwong-Soave model was used to estimate the properties of the gases (Cormos et al., 2021; Ghanbari et al., 2017; Tilak and El-Halwagi, 2018). The properties of the solids —heat capacity, enthalpy,

entropy, and energy— were calculated with the Barin equations (Aspen Technology, Inc., 2001; Barin, 1995).

For the modeling of the IHCaL loop, the same approach as in the work of Greco-Coppi et al. (2023) was used. The make-up input and the purge were located at the calciner input and the calciner output, respectively. The composition of the limestone used for all the processes was assumed to be equivalent to the composition of the raw material of the lime plant, displayed in Table 4.

To achieve fluidization, CO_2 is recirculated from the calciner exit back into the inlet. The amount of fluidizing agent required ($F_{CO2,rec}$) is calculated with the assumptions presented by Greco-Coppi et al. (2023). Since $F_{CO2,rec}$ both depends on and influences the calciner heat requirement, these two quantities are calculated by solving the whole mass and energy balances iteratively until the relative variation of $F_{CO2,rec}$ is less than 10%.

Table 4. Composition of the limestone from the host lime plant, used as raw material and as make-up for the IHCaL process. Adopted from Greco-Coppi et al. (2021).

Component	Mass fraction
$CaCO_3$	98.3 %
$MgCO_3$	0.7 %
SiO_2	0.7 %
Fe_2O_3	0.1 %
Al_2O_3	0.2 %
SO_3	<0.1 %

For the calcination of $CaCO_3$, a conversion of 99% in the calciner was assumed. The deactivation of the sorbent was calculated considering the carbonator and the calciner as perfectly stirred reactors, with a model described elsewhere (Abanades et al., 2005; Abanades, 2002). The active fraction of CaO entering the carbonator ($X_{ave,max}$) is obtained with Eq.(3).

$$X_{ave,max} = \frac{f_m(1-f_w)F_0}{F_0 + F_R(1-f_m)} + f_w \quad (3)$$

Here, the values of the fitting constants reported by Abanades and Alvarez (2003) for natural limestone were adopted: f_m=0.77 and f_w=0.17. This model was programmed into a FORTRAN routine in the Aspen Plus® process model. For the computation of the CO_2 absorption, the hydrodynamics of the carbonator were simulated with models from Kunii and Levenspiel (1991) and the reaction kinetics were modeled following Abanades et al. (2004). The solid circulation (Φ) was varied until a capture efficiency (E_{cc}) of 90% was achieved with less than 0.05% absolute error. A detailed description of the carbonator reactor model can be found in the work of Lasheras et al. (2011). The main model assumptions were adopted from Greco-Coppi et al. (2023).

The main assumptions affecting the power requirements in the IHCaL process are displayed in Table 5. The power requirement calculations were performed with the Aspen Plus® models. The

CO_2 compression represents the highest power input. The electric power consumption for circulation of the flue gases and propelling of the fluidization agents is also taken into account.

Table 5 Main assumptions and general input parameters for the calculation of power requirements with values form Greco-Coppi et al. (2023)

CO_2 Compression	**Value**
Number of stages *	5
Temperature after intercooler (°C)	25
Pressure drop intercooler (mbar)	100
Polytropic efficiency (%)	80
Mechanical efficiency (%)	95
Discharge conditions	
Temperature (°C)	25
Pressure (bar_a)	110
Inlet conditions	
Temperature (°C)	25
Pressure (bar_a)	1.013
Blowers of the IHCaL Facility	**Value**
Mechanical efficiency (%)	90
Isentropic efficiency (%)	65
Δp_{carb} (mbar)	100
Δp_{calc} (mbar)	130
Δp_{comb} (mbar)	150
$u_{0,calc}$ (m/s)	0.25
$T_{FA,carb}$ (°C)	250
$T_{FA,calc}$ (°C)	450

* Equal pressure ratio

2.4. Process Key Performance Indicators

The process key performance indicators (KPIs) were defined based on the work of Anantharaman et al. (2018).The capture efficiency (E_{CC}) is defined as the ratio of captured CO_2 to the total CO_2 generated, including the kiln —for the tail-end configurations—, and the IHCaL combustor and calciner. It can be calculated with Eq.(4), considering the molar flow rate of CO_2 leaving the carbonator (not captured) and the molar flow rate of CO_2 leaving the calciner (captured). Herby, it is assumed that no CO_2 slip occurs.

$$E_{CC} \equiv \frac{\{Captured\ CO_2\}}{\{Generated\ CO_2\}} = \left(1 + \frac{F_{CO2}^{carb}}{F_{CO2}^{calc}}\right)^{-1} \tag{4}$$

It is useful to define normalized values of the heat and the production to evaluate the performance of the capture facility. The absolute heat ratio (HR_a) is the quotient of the total heat input in the new concept, $\dot{Q}_{in}$, and the heat requirement of the reference facility, $\dot{Q}_{in}^{ref}$. The (specific) heat ratio (HR) is the ratio of specific heat requirement per ton of produced lime. The product ratio is the ratio of product mass flow in the new concepts to the production of the

reference facility. These quantities are defined mathematically in Eq.(5), where $\dot{m}_{CaO}$ is the mass flow of product flow rate.

$$HR_a \equiv \frac{\dot{Q}_{in}}{\dot{Q}_{in}^{ref}} \quad HR \equiv \frac{\dot{Q}_{in} / \dot{m}_{CaO}}{\dot{Q}_{in}^{ref} / \dot{m}_{CaO}^{ref}} \quad PR \equiv \frac{\dot{m}_{CaO}}{\dot{m}_{CaO}^{ref}} \tag{5}$$

For the calculation of *HR* and HR_a, it was assumed that the purge from the IHCaL process can be sold as product. There is evidence in the literature that supports this assumption. Dean et al. (2013), Telesca et al. (2014), Telesca et al. (2015), and Hills (2016) studied the utilization of carbonate looping purged sorbent in the cement industry. Their results suggest that this kind of integration would be possible. Furthermore, the results from the sorbent analysis of the IHCaL pilot plant operation at the technical university of Darmstadt (Hofmann et al., 2022b; Ströhle et al., 2021) show that purge samples have similar properties to commercial lime, especially in terms of reactivity. These results will be reported and discussed in a later publication.

To evaluate the heat recovery with the steam cycle, a new KPI is defined, namely the heat-to-power ratio (*HtPR*). The *HtPR* is the quotient of the net generated power in the steam cycle to the heat input in the IHCaL combustor, and can be calculated with the following equation:

$$HtPR = \frac{P_{el,SC}}{\dot{m}_{fuel}^{comb} \cdot LHV} \tag{6}$$

Where, $P_{el,SC}$ is the net power of the steam cycle in MW_e —without subtracting the power requirement of the capture facility for the blowers and the compression—, $\dot{m}_{fuel}^{comb}$ is the mass flow input of fuel in the combustor, and LHV is the corresponding lower heating value.

To evaluate the heat and energy utilization, the specific primary energy consumption for CO_2 avoided (*SPECCA*) was calculated according to Eq.(7).

$$SPECCA = \frac{q - q^{ref}}{e_{CO2}^{ref} - e_{CO2}} \tag{7}$$

Here, *q* and e_{CO2} are the specific primary energy consumption and the specific CO_2 emissions, respectively. *q* is obtained considering the direct primary energy consumption from the fuel input and the indirect primary energy consumption related to the net power requirement (P_{el}), according to Eq.(8).

$$q = \frac{\dot{m}_{fuel} \cdot LHV + P_{el} / \eta_{ref,el}}{\dot{m}_{CaO}} \tag{8}$$

Here, a reference electrical efficiency of the grid ($\eta_{ref,el}$) should be assumed. For the computation of the specific emissions, the direct CO_2 emissions from the combustion and calcination are considered, as well as the indirect CO_2 emissions associated with the electric power. The following equation is used to calculate this parameter:

$$e_{CO2} = e_{CO2,d} + \frac{P_{el}}{\dot{m}_{CaO}} \cdot e_{ref,el} \tag{9}$$

$e_{ref,el}$ is the CO_2 emissions factor of the electricity mix considered, and $e_{CO2,d}$ are the direct fossil CO_2 emissions per unit of product. $e_{CO2,d}$ can be calculated from the fossil CO_2 generation rate ($\dot{m}_{CO2,foss}$) and the CO_2 capture rate ($\dot{m}_{CO2,capt}$) with Eq.(10).

$$e_{CO2,d} = \frac{\dot{m}_{CO2,foss} - \dot{m}_{CO2,capt}}{\dot{m}_{CaO}} \quad (10)$$

For all the calculations, different energy scenarios were assumed to assess the variability of the results with the efficiency and the reference emissions factor of the energy mix. The corresponding assumptions were adopted from Anantharaman et al. (2018), and are presented in Table 6. Here, EU-28 is the European energy mix calculated for the year 2015, and NGCC means "natural gas combined cycle".

Table 6. Energy scenarios for the SPECCA calculations, based on data from Anantharaman et al. (2018).

Number	Energy scenario (ES)	$\eta_{ref,el}$ (%)	$e_{ref,el}$ (kg_{CO2}/MWh)
ES-1	EU-28* energy mix (2015)	45.9	262
ES-2	Coal, state-of-the-art	44.2	770
ES-3	Coal, sub-critical	35.0	973
ES-4	NGCC†	52.5	385
ES-5	Renewables	100	0
ES-6	Nuclear	33.0	0

*EU-28: European Union; †NGCC: Natural gas combined cycle

2.5. Economic Model

The economic analysis was performed with the ECLIPSE modeling and simulation software (Ulster University, 1992; Williams and McMullan, 1996). ECLIPSE is a program developed by Ulster University with the aim of seamlessly merging the process modeling and the economic assessment, thus enabling the complete techno-economic assessment (TEA) within a single software suite. It has been widely used in the last years to assess the economic performance of different technologies, including CO_2 capture processes (Dave et al., 2013; Huang et al., 2018; Rolfe et al., 2018b; Rolfe et al., 2018a). A detailed description of the ECLIPSE model and its validation is given in Williams and McMullan (1996), while an overview of ECLIPSE is included herein.

The ECLIPSE program structure is shown in Figure 7. ECLIPSE requires user input to define and specify the process. This includes the process flow diagram and relevant technical data. Other information is read from the embedded databases. There are three databases used by ECLIPSE: compound, utilities, and cost. They are continuously updated and expanded, taking into account the specific needs of the project studied and incorporating data from industrial partners, the project itself, and the literature.

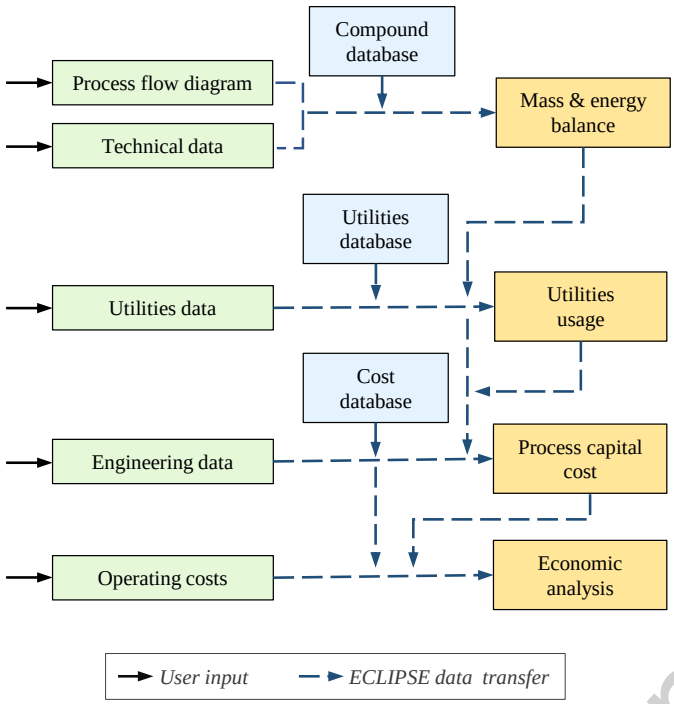

Figure 7. ECLIPSE Program Structure adapted from Williams and McMullan (1996) with permission from John Wiley and Sons.

Once the process flow diagram and technical data is input into ECLIPSE, the mass and energy balance is calculated. ECLIPSE transfers the results along with user input utilities data and database information, to determine the utilities usage (electricity, water, etc.,) for the process. The data on utilities usage is then applied in the capital cost estimation, incorporating user input engineering data and information from the cost database. Finally, the economic analysis is completed using the cost database and previously determined capital cost data, as well as operating costs.

The economic analysis consists of estimating the capital and operating costs, as well as giving an indication of the convenience of the investment based on the net present value (NPV) approach (Huang, et al., 2013). There are three stages to the economic analysis: (i) determination of the fixed process capital costs, and process utility capital cost; (ii) determination of the operation and maintenance (O&M) costs; and (iii) economic assessment. The Chemical Engineering Plant Cost Index (CEPCI) is used to normalize the data and the results to the year 2020 (Chemical Engineering, 2023; Mignard, 2014).

The calculation of initial capital costs (initial CAPEX, i.e. I_0) is performed using the two approaches illustrated in Figure 8. For standard equipment (i.e., market-available equipment), manufacturers' quotes, published prices in literature, and historical project data are used (see Figure 8, right branch). If the capital cost of similar components but with a different size or capacity is known, the capital cost is scaled up or down using the correlation given in Eq.(11) (Gogulancea et al., 2023).

$$Cost = Cost_{ref}\left(\frac{Size}{Size_{ref}}\right)^{Factor} \quad (11)$$

Where $Cost_{ref}$ is the reference cost of equipment of capacity $Size_{ref}$, and *Cost* is the approximate cost of equipment with a corresponding capacity *Size*. *Factor* is the value of the scaling exponent, which ranges from 0.6 to 0.8 for most components (Gogulancea et al., 2023).

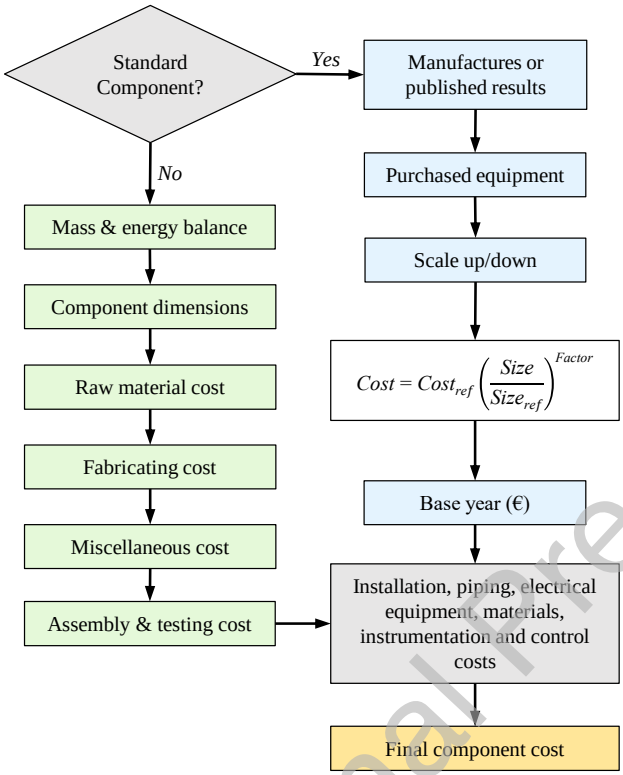

Figure 8: Methodology for capital cost estimation of standard and non-standard components.

For non-standard equipment, a bottom-up cost approach based on the mass and energy balances within the ECLIPSE simulation is adopted. This approach is illustrated in the left branch of Figure 8. It involves the dimensioning of the components with the results from the mass and energy balance; the estimation of the raw material, fabrication, and miscellaneous costs; and the addition of the assembly and testing costs.

After the estimation of the equipment costs, each individual cost is expanded by an allowance for installation and integration, such as piping, valves, instrumentation, and civil work (see last two blocks in Figure 8), thus obtaining the final component costs. The absolute accuracy for an individual unit, for this type of capital cost estimation procedure, is estimated at about ± 25–30%. Since the concepts assessed consist of similar types of equipment, the analysis maintains a consistent basis, ensuring comparability of results (cf. Wang et al., 2006).

Operation and maintenance (O&M) costs include (i) annual capital expenditure (CAPEX) for spares, maintenance, and plant replacement; (ii) fixed operating expenditure (OPEX) for labour, overhead, and insurance; and (iii) variable OPEX for consumables, such as fuel and limestone.

These costs are based on the mass and energy balances produced within the ECLIPSE software, and the stream costs specified by the user (Williams and McMullan, 1996). While technically the electricity export is a variable OPEX, it is reported as a separate element for clarification purposes. An annual miscellaneous cost category is also included for the remaining expenses, i.e. facility supplies, building extension, power transformer upgrading, chemicals, and other regular operating costs.

The final step consists in the economic assessment, considering the overall process investment (I_0), together with the individual input streams, and the O&M costs. With all the costing results, the annual cash flow and the breakeven selling price (*BESP*) of lime (product) are calculated (see Section 2.6). Additionally, a sensitivity analysis is performed to disclose the effect of dominant parameters, such as energy cost, feedstock price, plant capacity factor, and fixed OPEX.

The main economic assumptions and relevant conditions for this work are shown in Table 7. The minimum and maximum columns were used as boundaries for the sensitivity analysis. The engineering, procurement, and construction (EPC) costs were attained via summation of the fixed process capital costs, the process utility capital costs, and the balance of plant costs. Unfortunately, due to commercial sensitivities, these values cannot be published. The initial capital expenditure (I_0) was determined by considering the owner's costs, which include working capital, capital fees, and commissioning costs, as well as the EPC. The owners' costs were determined as a percentage of the EPC[1].

[1] This is a similar methodology to the one presented by Roussanaly et al. (2017). They use a slightly different nomenclature and grouping of the subtotals. In their work, the total plant costs (TPC) are determined by multiplying the EPC by a factor, and the EPC are calculated by multiplying the total direct costs (TDC) by another factor.

Table 7: Boundary conditions for the economic assessment

Category	Parameter	Min.	Baseline	Max.	Unit
Economic Parameters	Contingency	10	15	20	% of EPC
	Discount rate (r)	4	6	8	%
	Plant life	20	25	30	years
	Construction time		2		years
	Interest rate during construction period		3		%
	Plant operating hours		8000		hours
	Payment schedule, year 1		40		%
	Payment schedule, year 2		60		%
Initial CAPEX (I_0)	**EPC**	Undisclosed due to commercial sensitivities			
	Fixed process capital costs				
	Process utility capital costs				
	Balance of plant				
	Owner's costs				
	Working capital		2		% of EPC
	Capital fees		1		% of EPC
	Commissioning costs		1		% of EPC
Annual CAPEX	Annual maintenance costs inc. labour & supplies		3.5		% of I_0
OPEX	**Fixed OPEX**				
	Annual insurance costs		1.5		% of I_0
	Annual operating costs inc. labour & supplies		3		% of I_0
	Variable OPEX				
	Lignite	0.96	1.2	1.44	€/GJ
	SRF	-48	-40	-32	€/ton
	Limestone		4		€/ton
	Electricity import*		120		€/MWh
	Electricity export		60		€/MWh

*Eurostat (2022)

2.6. Economic Key Performance Indicators

For the economic analysis, the key performance indicators are the break-even selling price (*BESP*) and the CO_2 avoidance cost (*CAC*). Due to commercial sensitivity, the return on investment (ROI) is not disclosed in this work.

The *BESP* is the price that the lime must sell for to cover all associated lifetime costs, i.e., the lime price that makes NPV = 0 at the end of the plant life. The *BESP* for each plant configuration and fuel type is calculated and compared to the reference plant. If the *BESP* is too high, then the plant may not be economically competitive, as the selling price required to recover costs and

return a reasonable profit on the investment may be too great in comparison to the average market selling price. The BESP can be calculated using Eq.(12):

$$BESP = \frac{\sum_{t=1}^{n} \frac{I_t + M_t + F_t}{(1+r)^t} + I_0}{\sum_{t=1}^{n} \frac{L_t}{(1+r)^t}} \tag{12}$$

Where I_t is the investment expenditure in year t (annual CAPEX), M_t is the O&M expenditure in year t, F_t is the fuel expenditure in year *t*, L_t is the quantity of lime produced in year *t*, *r* is the discount rate, I_0 is the initial investment (CAPEX), and *n* is the system life.

For the impact of CO_2 capture on the plant economics, the CO_2 avoidance costs (*CAC*), Eq.(13), are calculated. The *CAC* is based on the reduction of CO_2 emissions per unit of the net product produced (Roussanaly, 2019; Simbeck and Beecy, 2011).

$$CAC\left(\mathrm{EUR/t_{CO2,av}}\right) = \frac{BESP_{capture} - BESP_{ref}}{CO_{2,emissions,ref} - CO_{2,emissions,capture}} \tag{13}$$

In general, the emissions are computed regardless of their biogenic or fossil origin throughout this work. Nevertheless, for the *CAC*, the economic benefit of CDR was also calculated by treating the captured biogenic CO_2 emissions as negative in Eq.(13) for the scenarios with SRF (see Figure 15). Costs for CO_2 transport and storage were excluded from the calculations.

3. RESULTS AND DISCUSSION

In this chapter, the results are discussed in two separate sections. The first section corresponds to the results of the process model, including the steam cycle, and the second section reports the results of the economic analysis.

3.1. Process Analysis

Three different heat recovery concepts for the high temperature (1000 °C) combustor flue gases were analyzed (see Figure 5). These concepts consisted in recovering heat only through combustion air preheating (I), recovering heat with a steam cycle before air preheating (II), and recovering heat into the steam cycle after air preheating (III). The optimal configuration of the corresponding steam cycles includes feedwater preheating, and superheating of steam up to 565 °C and 130 bar. Apart from the heat recovery from the combustor flue gases, heat is recovered from the carbonator cooling system, the carbonator flue gases, and the calciner flue gases. Recovering heat from the combustor flue gases is detrimental to the thermodynamics of the entire process, but it may be used to decrease the operating temperature of some components (e.g., filters and blowers), and thus reduce costs. From the heat input into the IHCaL process, up to ca. 80% can be recovered in a steam cycle to produce electricity with a net electric efficiency of 41–42%. This value is lower than values reported in the literature for power plants, due to the smaller size of the steam cycle and the capture facility. For example, Hawthorne et al. (2009)

reported a net power efficiency of 45.3% for the steam cycle associated with a 1599 MW_{th} CaL unit.

If waste-derived fuels are used in the combustor, chlorine-aided corrosion may be an issue for the system. One way to evaluate this is with the aid of the Flingern diagram (Haider et al., 2008), which takes its name from the incineration facility in Düsseldorf-Flingern. In this facility, the influence of the flue gas temperature and the superheater temperature in the corrosion was quantified during the 1970s (Haider et al., 2008). The diagram that resulted from the empirical investigations establishes limits for three operating regimes, categorized according to the probability of corrosion —namely, minimum corrosion, moderate corrosion, and high corrosion.

The analysis of the corrosion limits with the Flinger diagram is illustrated in Figure 9 for the concepts in which combustor flue gases are cooled down by superheating or reheating steam. In the integrated concept (III), the superheater (SH2) operates below the corrosion limit because the flue gases from the combustor are cooled down by the air preheater before recovering heat through the steam cycle. Hence, the integrated concept (III) is suitable for operation with waste-derived fuels, such as SRFs, from the point of view of the low corrosion risk.

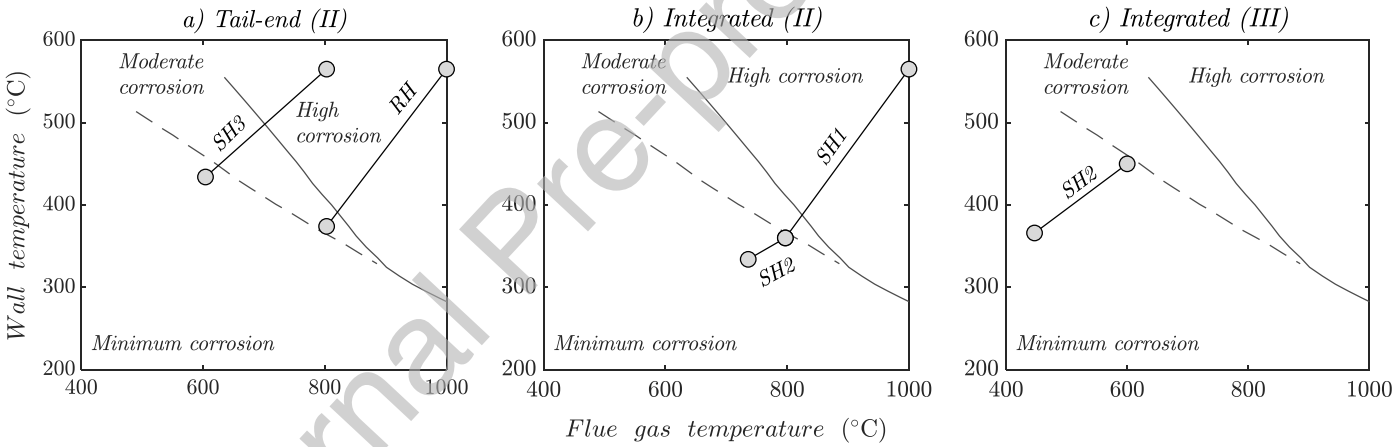

Figure 9. Flingern diagram for the heat recovery from combustor flue gases when firing waste-derived fuels. The corrosion limits were adopted from Warnecke (2004).

The tail-end concept (II) and the integrated concept (II) have heat exchangers operating in the high corrosion regimes. The reasons for this are the high temperature of the combustor gases at the point of heat recovery, and the configuration of the steam cycle. Corrosion problems are to be expected with these arrangements if the combustor is fueled with waste-derived-fuels.

To mitigate corrosion issues, different strategies may be adopted. One option would be to use the combustor flue gases to exchange heat with an evaporator instead of (or before) a preheater or superheater. This would lower the wall temperature of the heat exchanger, displacing the operation regime towards a less problematic regime in terms of corrosion. Another strategy, which was not computed in this work, but may be useful in some applications would be to cool down the flue gases by preheating the sorbent make-up streams, thus reducing the temperature of the flue gas, while recovering heat for the capture process. Reducing the temperature of the live steam may also reduce corrosion problems, but would impact the efficiency of the steam cycle negatively. Finally, a combination of the strategies proposed could give an optimal solution in

terms of achieving a compromise between minimizing the corrosion issues and maximizing the power output of the steam cycle.

Notwithstanding the foregoing, it is worth pointing out that the corrosion issues in the IHCaL process may also arise inside the combustor, where the metallic heat pipes lay for the heat transfer to the calciner. Considering the high temperature of operation (ca. 900°C), high concentrations of Chlorine should be avoided to metallic components (mainly the heat pipes). Chlorine flue gas concentrations higher than 600 ppm (Qu et al., 2020) should be avoided for the combustor, which limits the selection of waste-derived fuels in terms of chlorine content.

The main results from the process modeling are shown in Table 8. In the tail-end solution, the use of SRF instead of lignite reduces the energy consumption for the configuration (I). This is due to the lower CO_2 emission factor of this fuel. For the configuration (II), the trend is reversed. This is because, in this configuration, less preheating of the combustion air is possible. Preheating is more critical for SRF, because of the higher air input requirement. This effect prevails over the reduction in heat requirement due to the lowest $e_{CO2,fuel}$.

Table 8. Main results of the process modeling

Configuration	**Tail-end**				**Fully integrated**					
Fuel	**Lignite**		**SRF**		**Lignite**			**SRF**		
Heat recovery	**I**	**II**	**I**	**II**	**I**	**II**	**III**	**I**	**II**	**III**
E_{cc}	90%	90%	90%	90%	90%	90%	90%	90%	90%	90%
$Q_{in,comb}$ (MW_{th})	121	174	119	178	46	62	59	46	62	57
Φ	5.40	5.37	5.55	5.60	1.36	1.68	1.64	1.30	1.60	1.52
Λ	0.10	0.10	0.10	0.10	1.20	0.89	0.93	1.30	0.96	1.05
$\eta_{net,SC}$	42.4%	43.4%	42.4%	43.4%	41.2%	41.3%	42.4%	41.2%	41.3%	42.4%
HRa	4.17	5.56	4.12	5.67	1.20	1.62	1.55	1.21	1.63	1.50
HR	3.03	3.79	3.03	3.89	1.20	1.63	1.55	1.21	1.63	1.50
PR	1.38	1.47	1.36	1.46	1.00	1.00	1.00	1.00	1.00	1.00
HtPR	32.9%	38.8%	32.9%	38.8%	16.8%	17.0%	24.8%	16.8%	17.0%	24.8%
$Q_{in,SC}$ (MW_{th})	94.0	155.7	92.7	159.5	18.7	25.5	34.6	18.8	25.7	33.5
P_{gross} (MW_e)	40.8	68.9	40.2	70.6	7.9	10.8	15.0	7.9	10.9	14.5
P_{net} (MW_e)	39.8	67.6	39.3	69.2	7.7	10.5	14.7	7.7	10.6	14.2
η_{net}	42.4%	43.4%	42.4%*	43.4%*	41.2%	41.3%	42.4%	41.2%*	41.3%*	42.4%*

*Assumption

For the integrated arrangement, the heat requirement is almost independent of the fuel type for the configurations (I) and (II). For the configuration (III), the solution with SRF is associated with a 3% reduction in the heat requirement compared with the lignite-fired concept. This is because of the relatively high amount of flue gases from the combustion of SRF compared to lignite, which allows heating up the combustion air up to higher temperatures. The ratios of flue gas to air are 112% and 115% for lignite and SRF, respectively. Overall, outside of these small differences, the variation of the heating requirement with the fuel type are negligible for all the cases considered. This is mainly because the main parameters of the fuels, *LHV* and $e_{CO2,fuel}$,

mutually compensate for their effects —higher *LHV* (as in lignite) and lower $e_{CO2,fuel}$ (as in SRF) reduce the heat requirements.

The circulation rate and the make-up rate have an important influence on the heat requirement of the process. For the tail-end solution, the make-up is given as an input, namely $\Lambda = 0.10$. In this configuration, higher circulation rates are required with SRF because less CO_2 from make-up is being calcined in the calciner; thus, higher capture rates in the carbonator are necessary to achieve the same overall capture efficiency. For the fully integrated concepts, the trend is reversed as the SRF generates less CO_2 and, since the mass flow rate of make-up is fixed, there is higher sorbent activity, which means that less circulation of sorbent is required.

The heat to power ratio (*HtPR*) is higher for the tail-end concepts (31–35%) because more heat is required for the capture than in the integrated solutions. This heat can be recovered in a steam cycle. For the integrated configuration, less power is generated (*HtPR* between 16 and 25%) because the heat is more efficiently used for the regeneration of the sorbent.

The formation of CO_2 is illustrated in Figure 10. Here, only the generation of CO_2 is considered, i.e., the capture is not displayed. The CO_2 formation is classified in four categories: (i) kiln, for the process and fuel emissions from the PRK; (ii) make-up, for the CO_2 formed from the calcination of limestone in the capture facility; (iii) fuel (fossil), for the fossil CO_2 produced in the IHCaL combustor; and (iv) fuel (bio), for the biogenic CO_2 formed by the combustion of fuel in the IHCaL plant. For the tail-end configurations, the additional CO_2 associated with the capture is higher than the original CO_2 formation. This is particularly critical for the lignite-fueled cases, where all the formation is fossil CO_2. When utilizing SRF in the IHCaL combustor, the increase of fossil CO_2 formation is less than the original CO_2 from the rotary kiln. For the fully integrated configurations, the total formation is almost equal to the emissions from the rotary kiln for all the cases, meaning that the capture facility does not significantly increase the CO_2 formation.

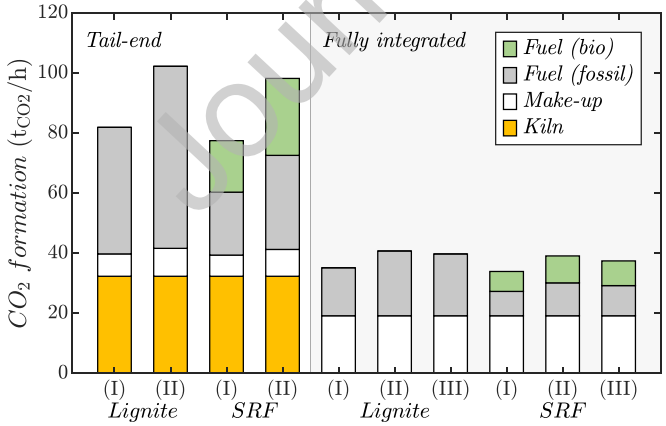

Figure 10. CO_2 formation breakdown for all the scenarios considered in the process model

The specific flow of energy for the different concepts is shown in Figure 11, broken-down according to the destination of the energy. Here, the categories are (i) calcination, for the energy used in the reaction to form CaO, (ii) power generation, for the net energy recovered in the steam cycle, and losses from the (iii) steam cycle and the (iv) capture process. The majority of the steam cycle losses are associated with the heat leaving the system through the condenser —due to thermodynamic limitations (law of entropy). For all the capture scenarios, there is an increase in the direct specific heat requirements due to the losses in the IHCaL process. The steam cycle configurations (I) are optimal from the point of view of reducing the fuel requirements but have less capacity to generate power. The integrated configurations have fewer specific requirements because of the efficient indirectly heated calcination in the calciner and the low amount of circulating sorbent.

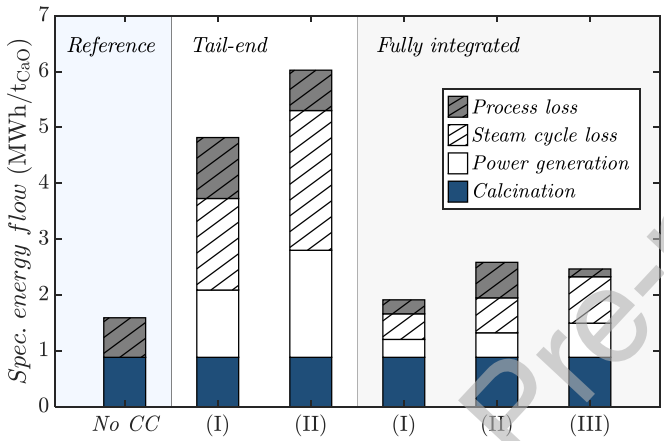

Figure 11. Specific energy flow for the reference lime plant and for the different scenarios considered in the process modeling.

The results of the *SPECCA* calculations for all the process configurations with carbon capture are displayed in Figure 12. Here, the energy scenarios ES-1 and ES-4 were used for the calculations[2]. The height of the bars indicate the mean *SPECCA* values, while the error bands corresponds to plus-minus one standard deviation of the corresponding results. The detailed results are included in Table 9.

The calculated values are relatively low, compared to other technologies (Voldsund et al., 2019). The reason for this is the efficient energy utilization enabled by the high temperatures and the net power production. The values for the fully integrated scenarios are particularly low due to the better heat utilization associated with the indirect calcination of limestone. Among the integrated configurations, the recovery strategies (I) and (III) performed better than (II). This is mainly due to the harnessing of the process heat, which was less effective for approach (II), as can be seen in the process losses illustrated in Figure 11.

[2] ES-5 and ES-6 were excluded from Figure 12 as they represent extreme cases rather than realistic energy mixes. The results from ES-1 to ES-4 are more representative of the process performance. For completeness, the full dataset is provided in Table 9.

The *SPECCA* results depend on the value assigned to the generated power; thus, since there is considerable power generation in all process configurations, there is high variability with the scenarios. Especially if the renewable (ES-5) and the nuclear (ES-6) energy scenarios are taken into account (see Table 9), extreme results are obtained, corresponding with the extreme values of the reference efficiency, $\eta_{ref,el}$. Overall, the results indicate that IHCaL technology is more attractive in energy scenarios with low renewable share and high CO_2 emissions associated with power generation. Depending on the local energy mix —considering also the expected variation during the lifetime of the capture project— a facility may be optimized for either power production (e.g., II), or reduced fuel requirement (e.g., I).

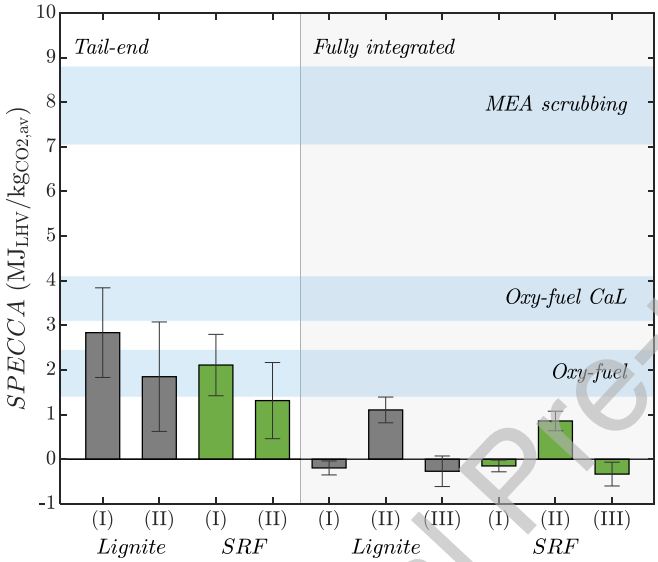

Figure 12. SPECCA results using energy scenarios ES-1 to ES-4. The bars show the mean values, and the error bands show the variation of plus-minus one standard deviation. Data for blue bands was obtained from Voldsund et al. (2019) for the same energy scenarios.

Table 9. SPECCA in $MJ_{LHV}/t_{CO2,av}$, for the process scenarios with CO_2 capture (S-2 to S-11), computed for different energy scenarios (ES).

Configuration	**Tail-end**				**Fully integrated**					
Fuel	**Lignite**		**SRF**		**Lignite**			**SRF**		
Heat recovery	**I**	**II**	**I**	**II**	**I**	**II**	**III**	**I**	**II**	**III**
ES-1	3.57	2.63	2.56	1.79	-0.15	1.26	-0.18	-0.11	0.97	-0.27
ES-2	2.53	1.50	1.95	1.15	-0.18	1.08	-0.24	-0.14	0.85	-0.30
ES-3	1.34	0.02	1.06	0.01	-0.44	0.65	-0.81	-0.36	0.51	-0.75
ES-4	3.91	3.25	2.86	2.30	-0.01	1.43	0.14	0.00	1.10	-0.01
ES-5	7.70	9.86	5.19	6.00	0.46	2.27	1.36	0.39	1.73	0.88
ES-6	1.87	-0.86	1.28	-0.53	-0.60	0.65	-1.32	-0.47	0.49	-1.12
Mean	3.49	2.73	2.49	1.79	-0.15	1.22	-0.17	-0.12	0.94	-0.26
Standard dev.	2.09	3.48	1.37	2.12	0.33	0.55	0.84	0.28	0.42	0.62

One of the main conclusions of this analysis is that the strategy for utilizing heat from the combustor flue gases is a key aspect for the integration. This is because of the high temperatures (≈1000°C) and the high amount of sensible heat associated. One of the strategies for integration (I) consists in recovering energy only through preheating of the combustor air. This increases the thermal efficiency of the IHCaL process but requires a gas/gas heat exchanger operating at high temperatures —up to 1000°C on the hot side, and up to 800°C on the cold side. Another possibility is to utilize this heat in a steam cycle (e.g., III). This may be a straightforward solution if lignite is fueled, but the design of the corresponding steam cycle would have to address chlorine-aided corrosion if waste-derived fuels are used. Preheating the make-up with combustor flue gases may be advantageous, especially for the fully integrated solutions that have high make-up rates. In this case, the system should be designed to avoid calcination before the entrance into the calciner. This last option was not investigated in this work.

3.2. Techno-Economic Analysis

The parameters for the cost calculation are shown in Table 7, and the year 2020 was taken as the reference for the price indexing. Table 10 shows the change in initial CAPEX (I_0) estimations for each of the plant configurations and fuels studied compared to the reference case. The tail-end cases tend to have larger I_0 than the fully integrated cases. This is due to the tail-end cases having greater solid circulation, as seen in Table 8, requiring larger plant sizes than the integrated cases.

Table 10: Percentage change in capital cost estimation compared to the reference case, for the scenarios with CO_2 capture (S-2 to S-11).

IHCaL integration	Fuel IHCaL combustor	Heat recovery concept*	Initial CAPEX increase against the reference case (%)
Tail-end	Lignite	I	367
		II	399
	SRF	I	367
		II	399
Fully integrated	Lignite	I	105
		II	112
		III	112
	SRF	I	105
		II	112
		III	118

*I: only air preheater; II: heat exchanger before air preheater; III: heat exchanger after air preheater

The breakdown of the annual operation and maintenance (O&M) costs are given in Figure 13. These include the annual costs for fuel and raw material costs, electricity revenue, end of pipe clean-up and waste disposal, as well as insurance, maintenance, and labor costs. The O&M costs for the integrated plants, for both fuel selections, are lower than for the tail-end plants. This is due to lower OPEX and CAPEX costs compared to the tail-end cases. The lignite integrated

plants also have lower fuel costs in line with the fuel requirements as per Table 8. For the lignite capture plants, the O&M costs are offset by revenue from electricity export. When lignite is replaced by the SRF, the O&M costs are offset by revenue from the electricity export and from SRF revenue —this is discussed in more detail in Section 3.2.2.

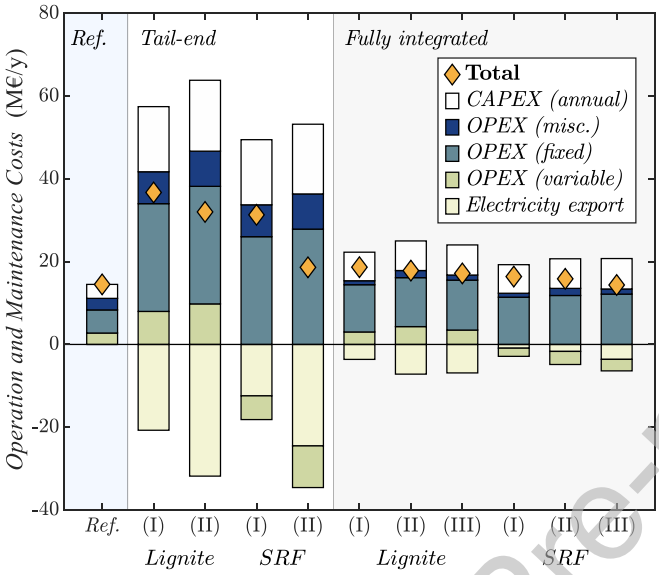

Figure 13: Annual operation and maintenance costs, for all the scenarios (S-1 to S-11).

Using the I_0 estimates, O&M costs, and the economic assumptions described in Table 7, the *BESP* for the lime product were calculated using the discounted cash flowrate analysis. The corresponding results are presented in Figure 14. Due to commercial considerations, the absolute value of the reference plant BESP has not been disclosed, and therefore, the BESP for the capture plants are presented in percentage change from the reference plant.

The techno-economic evaluation shows that for the lignite fueled plants, the fully integrated lignite (I) case has the highest *BESP*, which is a 45% increase compared to the base case. Cross-referencing this plant with the process modeling results in Table 8, it is shown that the fully integrated lignite (I) plant has the lowest thermal input of all the plants, and hence the lowest electricity export. Conversely, the lignite plant with the highest thermal input and electricity generation is the tail-end lignite (II) plant, which is also the lignite capture case with the lowest *BESP*, with only a 26% increase compared to the base case plant.

The same plant configurations have the highest and lowest *BESP* when the fuel is switched to SRF, however, the *BESP* is 33% and –14%, respectively, compared to the reference lignite plant. The tail-end SRF (II) plant is the only one with *BESP* value lower than the base case *BESP*. This is highly dependent on two revenue streams, electricity export, and SRF consumption. This plant has a large thermal input, which is fueled via the SRF, and has the greatest amount of heat recovery for electricity production and export, see Table 8.

Another point of note is that from Table 10 and Figure 13, the capital costs and O&M costs, are higher for the tail-end plants than for the integrated plants, yet the *BESP* is lower for the tail-end plants. As previously stated in Section 2.4, purge material from the tail-end IHCaL process can be sold as product; thus, the tail-end lime plants have increased lime output, and given that the *BESP* is calculated on per ton of product produced bases, the higher capital and O&M costs are absorbed by the higher lime output.

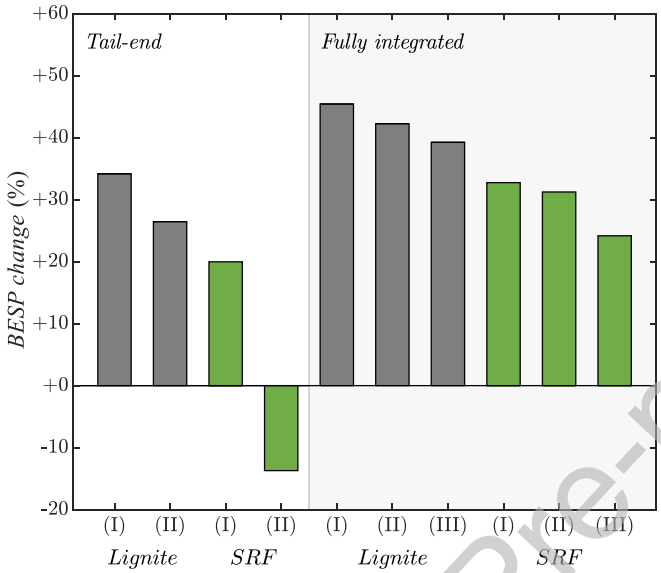

Figure 14. Lime plant BESP change compared to the reference case without carbon capture, for the scenarios with CO_2 capture (S-2 to S-11).

The CO_2 avoidance costs are shown in Figure 15. For the lignite plants, the CO_2 avoidance costs range from 20.39 to 34.3 €/$t_{CO2,av,}$ with the tail-end (II) case having the lowest cost of avoidance and the fully integrated (I) plant having the highest. These values are lower than what was reported by Santos and Hanak (2022), and De Lena et al. (2019).

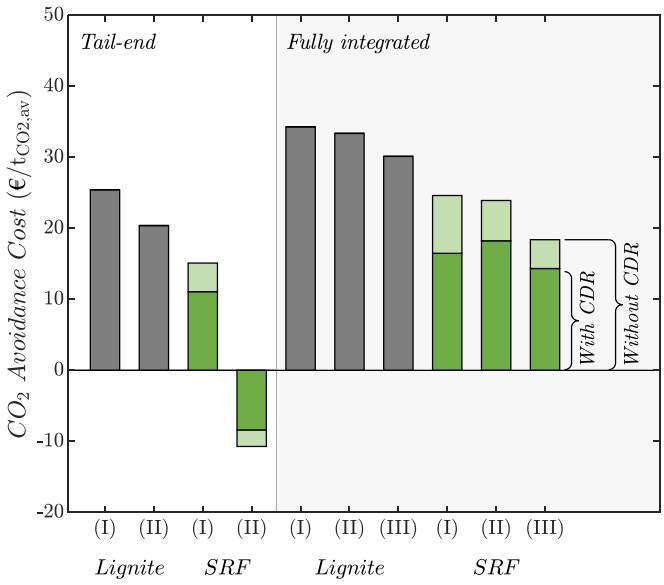

Figure 15. CO_2 Avoidance Cost (CAC) for the scenarios with CO_2 capture (S-2 to S-11).

For the SRF plants, the CO_2 avoidance range is -10.7 to 24.6 €/$t_{CO2,av}$, this is for the tail-end SRF (I) case and the fully integrated SRF (I) case, respectively, without computing negative emissions from captured biogenic CO_2. Again, electricity export has a large influence on the avoidance costs. Further to this, as already stated, the SRF plants attain additional revenue from utilizing this kind of fuel. As the tail-end SRF (II) plant consumes the largest quantity of SRF, it receives a higher value from this revenue stream, and hence the negative value.

The influence of CDR is illustrated in Figure 15. If negative CO_2 emissions are computed for the captured biogenic CO_2, net negative emissions are achieved in all the scenarios using SRF as fuel for the IHCaL. The *CAC* is reduced (excepting negative *CAC*) because of the higher amount of CO_2 avoided. If the economic benefit of CDR is considered, the avoidance costs are lower than 19 EUR/$t_{CO2,av}$ for all the scenarios analyzed.

3.2.1. Sensitivity Analysis

The influence of the main economic parameters on the *BESP* of lime produced has been investigated. The tail-end (I) and fully integrated (I) cases, fueled with lignite and SRF have been selected for the sensitivity study. The sensitivity parameters selected for the study include fuel price, project lifetime, discount rate (*r*), and contingency value. The results are shown in Figure 16 as relative change of *BESP* when the parameters are varied between the minimum and maximum boundaries from Table 7. For all lime plants, the discount rate (*r*) and project life are the main parameters that influence the *BESP*. Fuel price and contingencies have a lower impact on the *BESP*.

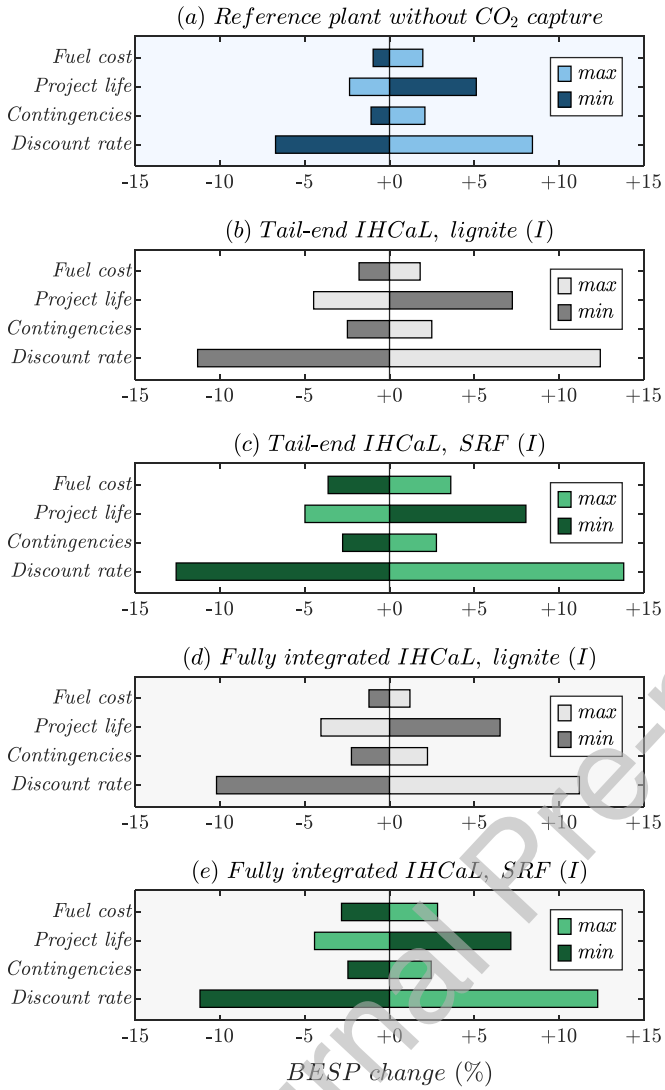

Figure 16. Results of the economic sensitivity analysis.

For the reference plant, increasing *r* from 6% to 8% increases the *BESP* by 8.4%, while decreasing *r* to 4% reduces the *BESP* by 6.7%. Increasing the project life to 30 years from 25 decreases the *BESP* by 2.4%, while decreasing the project life to 20 years increases the *BESP* by 5.1%. Increasing the contingency from 15% to 20% increases the *BESP* by 2.1%, and decreasing to 10%, decreases the *BESP* by 1.1%. Lastly, increasing the lignite price to 1.44 from 1.2 €/GJ increases the *BESP* by 2%, while decreasing the lignite price to 0.96 €/GJ decreases the *BESP* by 1%.

The tail-end lignite (I) configuration is more sensitive to variations than the reference scenario, increasing the *r* from 6% to 8% increases the *BESP* by 12.4%, while decreasing *r* to 4% reduces the *BESP* by 11.3%. Increasing the project life to 30 years from 25, decreases the *BESP* by 4.5%, while decreasing the project life to 20 years increases the *BESP* by 7.3%. Increasing the contingency from 15% to 20% increases the *BESP* by 2.5%, and decreasing to 10%, decreases

the *BESP* by 2.5%. Lastly, increasing the lignite price to 1.44 from 1.2€/GJ increases the *BESP* by 1.8%, while decreasing the lignite price to 0.96€/GJ decreases the *BESP* by 1.8%.

The integrated configuration, using lignite as fuel (S-6) is more sensitive to variations than the reference plant but less so than the tail-end plant. Increasing the *r* from 6% to 8% increases the *BESP* by 11.2%, while decreasing *r* to 4% reduces the *BESP* by 10.2%. Increasing the project life to 30 years from 25, decreases the *BESP* by 4%, while decreasing the project life to 20 years increases the *BESP* by 6.5%. Increasing the contingency from 15% to 20% increases the *BESP* by 2.2%, and decreasing to 10%, decreases the *BESP* by 2.2%. Lastly, increasing the lignite price to 1.44 from 1.2 €/GJ increases the *BESP* by 1.2%, while decreasing the lignite price to 0.96€/GJ decreases the *BESP* by 1.2%.

The same trends in key parameters are seen in the plants fueled by SRF. The tail-end SRF (I) case is more sensitive to economic parameters' variations than the reference case and the same plant fueled by lignite. Increasing the *r* from 6% to 8% increases the *BESP* by 13.8%, while decreasing *r* to 4% reduces the *BESP* by 12.6%. Increasing the project life to 30 years from 25, decreases the *BESP* by 5%, while decreasing the project life to 20 years increases the *BESP* by 8.1%. Increasing the contingency from 15% to 20% increases the *BESP* by 2.8%, and decreasing to 10%, decreases the *BESP* by 2.8%. Lastly, increasing the SRF price to 1.44 from 1.2€/GJ increases the *BESP* by 3.6%, while decreasing the lignite price to 0.96€/GJ decreases the *BESP* by 3.6%.

The fully integrated SRF (I) case is more sensitive to economic parameters' variations than the reference scenario and the same plant fueled by lignite, but less so than the tail-end SRF (I) plant. Increasing the *r* from 6% to 8% increases the *BESP* by 12.3%, while decreasing *r* to 4% reduces the *BESP* by 11.2%. Increasing the project life to 30 years from 25, decreases the *BESP* by 4.4%, while decreasing the project life to 20 years increases the *BESP* by 7.2%. Increasing the contingency from 15% to 20% increases the *BESP* by 2.5%, and decreasing to 10%, decreases the *BESP* by 2.5%. Lastly, increasing the SRF price to 1.44 from 1.2€/GJ increases the *BESP* by 2.8%, while decreasing the lignite price to 0.96€/GJ decreases the *BESP* by -2.8%.

Overall, the capture cases are more sensitive to variation than the reference case, and the tail-end cases more so than the integrated cases. The SRF fueled cases are more sensitive to variation than their counterpart fueled by lignite. The variation of the discount rate (*r*) has the greatest impact on the *BESP*, and the contingency and fuel price have similar impacts on the *BESP*.

3.2.2. Extended SRF Price Analysis

SRF is often a negative price; thus, the SRF producer pays the end-user to utilize SRF. Normal industrial waste collection procedures require a waste company to collect waste for a fee. The SRF producer collects the waste for a fee lower than the landfill tax (currently in England and Northern Ireland, £102.10 (119.16 €) per tonne (UK Government Digital Service, 2023). The waste is sorted and processed into SRF incurring a processing cost of around 15-20 €/t, this has thus far resulted in negative SRF prices.

Currently in the UK and Europe, SRF does not attract carbon tax, however, this is due to change in 2028 (Reeves et al., 2023). Furthermore, as demand for SRF increases and supply is limited by

production capacity, market forces for supply and demand have the potential to increase the price of SRF.

An extended sensitivity study has been done to consider the impact on the *BESP* for both lime plant IHCaL configurations with heat recovery strategy (I). The results are displayed in Figure 17. The SRF price ranges between -50 and +30 €/t and is benchmarked against the lignite for *BESP* for the same configurations. For the tail end option, an SRF price of approx. -20 €/t has an economic equivalence to the lignite-fueled plant. For the fully integrated plant, the lignite equivalence occurs when the SRF price is approx. -12 €/t. The crossover values would be higher if a profit were associated with CDR for the biogenic CO_2 from the combustion of SRF (cf. Figure 15).

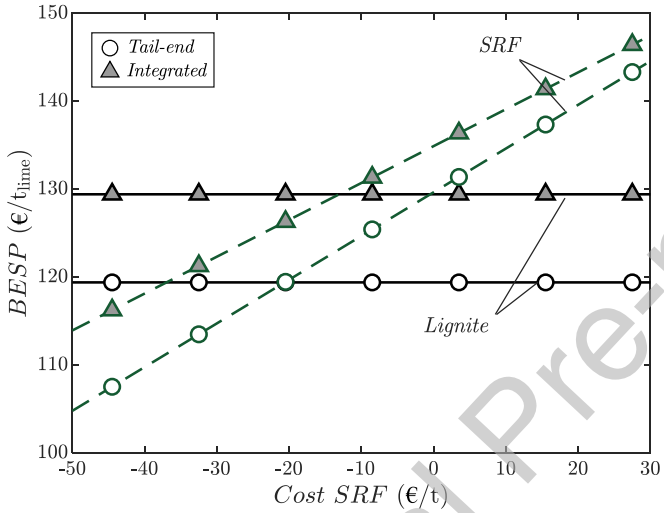

Figure 17: Extended sensitivity study on the SRF price

4. CONCLUSION

Within this work, ten different integrated concepts of the IHCaL process for the lime production were analyzed. A tail-end and a fully integrated configuration were studied in combination with various approaches to recover heat with a steam cycle. Furthermore, the corresponding technical implications of the integration options were discussed. The heat recovery strategy for the combustor flue gases was found to be a key factor to enable the deployment of the IHCaL technology.

For the tail-end solution, recovering heat from combustion flue gases allows for high recovery rate and substantial power production, but increases the fuel requirement by 44%. An efficient option to minimize the heat input in the combustor is to utilize the combustion flue gases only for the preheating of the flue gases. For the fully integrated configurations, recovering heat from combustion flue gases, downstream from the air preheater, is a reasonable strategy to increase the power output of the steam cycle (91% increase) with relatively low increase in the fuel demand (29% increase).

Relatively low values of specific primary energy consumption for CO_2 avoided (*SPECCA*) are achieved compared with values from other capture technologies reported in the literature for similar applications (De Lena et al., 2022; De Lena et al., 2019; Voldsund et al., 2019). Utilizing SRF gives better results than firing lignite but could lead to chlorine-aided corrosion in some configurations of the steam cycle. Additionally, negative *SPECCA* values are obtained for some fully integrated arrangements, which reveals the high efficiency of this kind of integration. Because of the considerable net power generation of the IHCaL concepts, there is a relatively high dependency of the results on the energy grid scenario assumed. The best results in terms of *SPECCA* are obtained for energy mixes with high CO_2 emissions associated with power generation, where the advantage of the net power injected to the grid is more significant.

The avoidance costs of the process scenarios with CO_2 capture are lower than the ones reported for other capture technologies for comparable applications (De Lena et al., 2019; Santos and Hanak, 2022). For all the plants considered, there are three possible avenues for revenue: (i) product sale, (ii) electricity export, and (iii) SRF utilization. The tail-end configurations produce additional lime in the downstream capture plants, which can be sold as product. This lowers the *BESP*, and the CO_2 avoidance costs.

Electricity generation, utilization, and export is key for favorable economics. Process scenarios with greater net electricity available for export have better economic results, such as lower *BESP* and CO_2 avoidance costs. However, they also entail higher heat requirements, leading to an increased fuel demand. In the tail-end SRF (II) case, the convergence of high electricity export and increased lime production leads to a lower *BESP* compared to the reference case. This, in turn, results in negative CO_2 avoidance cost (-10.7 €/$t_{CO2,av}$).

Utilizing waste-derived fuels in the IHCaL process has the potential to provide twofold economic benefits. On the one hand, it is a means of waste management, corresponding to the fourth policy in the hierarchy of the European legislation (European Union, 2018, 2008), thus enabling “negative costs” of fuel, associated with the added value of the disposal. On the other hand, net negative CO_2 emissions may be achieved, which, if marketed as credits from carbon dioxide removal (CDR), can further decrease the avoidance costs. In all the SRF scenarios analyzed throughout this work, CDR reduced the CO_2 avoidance costs by around 25% and the maximum costs were 18.2 EUR/$t_{CO2,av}$, excluding costs for transport and geological storage.

SRF is a finite resource, dependent on available waste streams and production capacity. The required specifications (e.g. impurities, heating value, and grain size distribution) may further limit the availability of suitable SRF. It is therefore reasonable to consider that the costs of this fuel may increase in the future, which would reduce the advantage of SRF over lignite.

The availability of lignite will decrease gradually in parallel to the closure of the German coal power plants until 2038. In line with this, it is necessary for lime producers to look for new fuel substitutes, such as SRFs, RDFs, and biomass-based fuels. This study presents one possible path to replace today’s fossil fuel utilization by an alternative fuel, namely SRF.

To push forward the IHCaL technology, some issues still need to be addressed. The sorbent calcination in the indirectly heated calciner of the IHCaL process requires further investigation. The IHCaL calciner did not perform as expected during the experimental pilot testing (Hofmann et al., 2024; Reitz et al., 2016), but the impact of the calciner performance in the CO_2 capture efficiency of the IHCaL system and the main factors affecting the calcination in the indirectly heated calciner are not yet fully understood.

Furthermore, there are still technical unknowns that can only be clarified with a scale-up of the IHCaL test rig. The next step towards industrial implementation of the technology by 2028 is the construction of a demonstration facility to capture CO_2 from flue gases of a cement or lime facility (Ströhle et al., 2021). This would enable the testing of a solid/solid heat exchanger to recover heat between the looped sorbent streams, and a high-temperature regenerative preheater for the combustion air. Additionally, the long-term operation of the demonstration plant would serve for the validation of the lifespan of the heat pipes heat exchanger in real operating environment, and the firing of waste-derived fuels in the combustor. Finally, the operation under low circulation rates and high make-up rates would validate the fully integrated concept.

ACKNOWLEDGEMENTS

The work leading to these results has received funding through the ACT program (Accelerating CCS Technologies, Horizon 2020 Project N° 294766) within the ANICA project. Financial contributions were made by the German Federal Ministry for Economic Affairs and Climate Action, the Department for Business, Energy and Industrial Strategy of the United Kingdom, and the Greek General Secretariat for Research and Technology. The support from Falah Alobaid in the design of the steam cycles and the assistance of Alina Greco Coppi in proofreading the article are greatly acknowledged as well.

CREDIT AUTHOR STATEMENT

Martin Greco-Coppi: Conceptualization, Methodology, Software (Aspen Plus®, EBSILON®*Professional*), Visualization, Writing – Original Draft (lead), and Writing – Review & Editing (lead). **Peter Seufert:** Writing – Original Draft (supporting), and Software (Aspen Plus®, EBSILON®*Professional*). **Carina Hofmann:** Writing – Review & Editing. **Angela Rolfe:** Methodology, Writing – Original Draft (economic assessment), and Writing – Review & Editing (economic assessment). **Ye Huang:** Software (ECLIPSE). **Sina Rezvani:** Writing – Review & Editing. **Jochen Ströhle:** Writing – Review & Editing, Supervision, Project Administration, and Funding Acquisition. **Bernd Epple:** Supervision and Funding Acquisition.

5. REFERENCES

Abanades, J.C., 2002. The maximum capture efficiency of CO_2 using a carbonation/calcination cycle of $CaO/CaCO_3$. Chemical Engineering Journal 90, 303–306. https://doi.org/10.1016/S1385-8947(02)00126-2.

Abanades, J.C., Alvarez, D., 2003. Conversion Limits in the Reaction of CO 2 with Lime. Energy Fuels 17, 308–315. https://doi.org/10.1021/ef020152a.

Abanades, J.C., Anthony, E.J., Lu, D.Y., Salvador, C., Alvarez, D., 2004. Capture of CO_2 from combustion gases in a fluidized bed of CaO. AIChE J. 50, 1614–1622. https://doi.org/10.1002/aic.10132.

Abanades, J.C., Anthony, E.J., Wang, J., Oakey, J.E., 2005. Fluidized bed combustion systems integrating CO_2 capture with CaO. Environmental science & technology 39, 2861–2866. https://doi.org/10.1021/es0496221.

Anantharaman, R., Berstad, D., Cinti, G., Gatti, M., 2018. D3.2 CEMCAP Framework for Comparative Techno-economic Analysis of CO_2 Capture from Cement Plants.

Andrew, R.M., 2018. Global CO_2 emissions from cement production. Earth Syst. Sci. Data 10, 195–217. https://doi.org/10.5194/essd-10-195-2018.

Arias, B., Diego, M.E., Abanades, J.C., Lorenzo, M., Diaz, L., Martínez, D., Alvarez, J., Sánchez-Biezma, A., 2013. Demonstration of steady state CO_2 capture in a 1.7MW_{th} calcium looping pilot. International Journal of Greenhouse Gas Control 18, 237–245. https://doi.org/10.1016/j.ijggc.2013.07.014.

Arias, B., Diego, M.E., Méndez, A., Abanades, J.C., Díaz, L., Lorenzo, M., Sanchez-Biezma, A., 2017. Operating Experience in la Pereda 1.7 MW_{th} Calcium Looping Pilot. Energy Procedia 114, 149–157. https://doi.org/10.1016/j.egypro.2017.03.1157.

Aspen Technology, Inc., 2001. Aspen Physical Property System: Physical Property Methods and Models V11.1. Cambridge, 436 pp.

Aspen Technology, Inc., 2020. Aspen Plus® V12 (38.0.0.380) [Computer software]. https://www.aspentech.com/en/products/engineering/aspen-plus.

Astrup, T., Møller, J., Fruergaard, T., 2009. Incineration and co-combustion of waste: accounting of greenhouse gases and global warming contributions. Waste management & research: the journal of the International Solid Wastes and Public Cleansing Association, ISWA 27, 789–799. https://doi.org/10.1177/0734242X09343774.

Baker, R.W., Freeman, B., Kniep, J., Huang, Y.I., Merkel, T.C., 2018. CO_2 Capture from Cement Plants and Steel Mills Using Membranes. Ind. Eng. Chem. Res. 57, 15963–15970. https://doi.org/10.1021/acs.iecr.8b02574.

Barin, I., 1995. Thermochemical data of pure substances, 3rd ed. VCH, Weinheim, 924 pp.

Böckh, P. von, Stripf, M., 2018. Thermische Energiesysteme: Berechnung klassischer und regenerativer Komponenten und Anlagen. Springer Vieweg, Berlin, Heidelberg, 276 pp.

Charitos, A., Rodríguez, N., Hawthorne, C., Alonso, M., Zieba, M., Arias, B., Kopanakis, G., Scheffknecht, G., Abanades, J.C., 2011. Experimental Validation of the Calcium Looping CO_2 Capture Process with Two Circulating Fluidized Bed Carbonator Reactors. Ind. Eng. Chem. Res. 50, 9685–9695. https://doi.org/10.1021/ie200579f.

Chemical Engineering, 2023. The Chemical Engineering Plant Cost Index. https://www.chemengonline.com/pci-home (accessed 19 November 2023).

Consonni, S., Viganò, F., 2012. Waste gasification vs. conventional Waste-to-Energy: a comparative evaluation of two commercial technologies. Waste management (New York, N.Y.) 32, 653–666. https://doi.org/10.1016/j.wasman.2011.12.019.

Cormos, A.-M., Dragan, S., Petrescu, L., Sandu, V., Cormos, C.-C., 2020. Techno-Economic and Environmental Evaluations of Decarbonized Fossil-Intensive Industrial Processes by Reactive Absorption & Adsorption CO2 Capture Systems. Energies 13, 1268. https://doi.org/10.3390/en13051268.

Cormos, C.-C., Dragan, S., Cormos, A.-M., Petrescu, L., Dumbrava, I.-D., Sandu, V., 2021. Evaluation of Calcium Looping Cycle as a Time-flexible CO_2 Capture and Thermo-Chemical Energy Storage System. Chemical Engineering Transactions 88, 19–24. https://doi.org/10.3303/CET2188003.

Da Cachola, C.S., Ciotta, M., Azevedo dos Santos, A., Peyerl, D., 2023. Deploying of the carbon capture technologies for CO2 emission mitigation in the industrial sectors. Carbon Capture Science & Technology 7, 100102. https://doi.org/10.1016/j.ccst.2023.100102.

Dave, A., Huang, Y., Rezvani, S., McIlveen-Wright, D., Novaes, M., Hewitt, N., 2013. Techno-economic assessment of biofuel development by anaerobic digestion of European marine cold-water seaweeds. Bioresource technology 135, 120–127. https://doi.org/10.1016/j.biortech.2013.01.005.

De Lena, E., Arias, B., Romano, M.C., Abanades, J.C., 2022. Integrated Calcium Looping System with Circulating Fluidized Bed Reactors for Low CO_2 Emission Cement Plants. International Journal of Greenhouse Gas Control 114, 103555. https://doi.org/10.1016/j.ijggc.2021.103555.

De Lena, E., Spinelli, M., Gatti, M., Scaccabarozzi, R., Campanari, S., Consonni, S., Cinti, G., Romano, M.C., 2019. Techno-economic analysis of calcium looping processes for low CO_2 emission cement plants. International Journal of Greenhouse Gas Control 82, 244–260. https://doi.org/10.1016/j.ijggc.2019.01.005.

Dean, C., Hills, T., Florin, N., Dugwell, D., Fennell, P.S., 2013. Integrating Calcium Looping CO_2 Capture with the Manufacture of Cement. Energy Procedia 37, 7078–7090. https://doi.org/10.1016/j.egypro.2013.06.644.

Diego, M.E., Arias, B., Abanades, J.C., 2016a. Analysis of a double calcium loop process configuration for CO_2 capture in cement plants. Journal of Cleaner Production 117, 110–121. https://doi.org/10.1016/j.jclepro.2016.01.027.

Diego, M.E., Arias, B., Méndez, A., Lorenzo, M., Díaz, L., Sánchez-Biezma, A., Abanades, J.C., 2016b. Experimental testing of a sorbent reactivation process in La Pereda 1.7 MW_{th} calcium looping pilot plant. International Journal of Greenhouse Gas Control 50, 14–22. https://doi.org/10.1016/j.ijggc.2016.04.008.

Dieter, H., Bidwe, A.R., Varela-Duelli, G., Charitos, A., Hawthorne, C., Scheffknecht, G., 2014. Development of the calcium looping CO_2 capture technology from lab to pilot scale at IFK, University of Stuttgart. Fuel 127, 23–37. https://doi.org/10.1016/j.fuel.2014.01.063.

Driver, J.G., Hills, T., Hodgson, P., Sceats, M., Fennell, P.S., 2022. Simulation of direct separation technology for carbon capture and storage in the cement industry. Chemical Engineering Journal 449, 137721. https://doi.org/10.1016/j.cej.2022.137721.

European Commission, H., 2020. Low Emissions Intensity Lime and Cement 2: Demonstration Scale. Leilac2 Project. https://doi.org/10.3030/884170.

European Union, 2008. Directive 2008/98/EC of the European Parliament and of the Council of 19 November 2008 on waste and repealing certain Directives. https://eur-lex.europa.eu/legal-content/EN/TXT/?uri=celex%3A32008L0098 (accessed 12 May 2023).

European Union, 2018. Consolidated text: Directive 2008/98/EC of the European Parliament and of the Council of 19 Consolidated text: Directive 2008/98/EC of the European Parliament and of the Council of 19 November 2008 on waste and repealing certain Directives. https://eur-lex.europa.eu/legal-content/EN/TXT/PDF/?uri=CELEX:02008L0098-20180705 (accessed 12 May 2023).

Eurostat, 2022. Electricity price statistics. https://ec.europa.eu/eurostat/statistics-explained/index.php?title=Electricity_price_statistics (accessed 15 December 2022).

Fan, L.-S., 2012. Separation of carbon dioxide from gas mixtures by calcium based reaction separation. https://patents.google.com/patent/us8226917/en.

Ferrari, M.-C., Amelio, A., Nardelli, G.M., Costi, R., 2021. Assessment on the Application of Facilitated Transport Membranes in Cement Plants for CO2 Capture. Energies 14, 4772.

Fu, C., Roussanaly, S., Jordal, K., Anantharaman, R., 2021. Techno-Economic Analyses of the CaO/CaCO3 Post-Combustion CO_2 Capture From NGCC Power Plants. Front. Chem. Eng. 2, 596417. https://doi.org/10.3389/fceng.2020.596417.

Furimsky, E., 2007. Carbon Dioxide Emission Index as a Mean for Assessing Fuel Quality. Energy Sources, Part A: Recovery, Utilization, and Environmental Effects 30, 119–131. https://doi.org/10.1080/15567030600820583.

Gardarsdottir, S., Lena, E. de, Romano, M., Roussanaly, S., Voldsund, M., Pérez-Calvo, J.-F., Berstad, D., Fu, C., Anantharaman, R., Sutter, D., Gazzani, M., Mazzotti, M., Cinti, G., 2019. Comparison of Technologies for CO_2 Capture from Cement Production—Part 2: Cost Analysis. Energies 12, 542. https://doi.org/10.3390/en12030542.

Gerassimidou, S., Velis, C.A., Williams, P.T., Komilis, D., 2020. Characterisation and composition identification of waste-derived fuels obtained from municipal solid waste using thermogravimetry: A review. Waste management & research: the journal of the International Solid Wastes and Public Cleansing Association, ISWA 38, 942–965. https://doi.org/10.1177/0734242X20941085.

Ghanbari, M., Ahmadi, M., Lashanizadegan, A., 2017. A comparison between Peng-Robinson and Soave-Redlich-Kwong cubic equations of state from modification perspective. Cryogenics 84, 13–19. https://doi.org/10.1016/j.cryogenics.2017.04.001.

Gogulancea, V., Rolfe, A., Jaffar, M., Brandoni, C., Atsonios, K., Detsios, N., Dieringer, P., Huang, Y., 2023. Technoeconomic and Environmental Assessment of Biomass Chemical Looping Gasification for Advanced Biofuel Production. Int. J. Energy Res. 2023, 1–17. https://doi.org/10.1155/2023/6101270.

Grasa, G.S., Abanades, J.C., 2007. Narrow fluidised beds arranged to exchange heat between a combustion chamber and a CO_2 sorbent regenerator. Chemical Engineering Science 62, 619–626. https://doi.org/10.1016/j.ces.2006.09.026.

Greco-Coppi, M., Hofmann, C., Ströhle, J., Walter, D., Epple, B., 2021. Efficient CO_2 capture from lime production by an indirectly heated carbonate looping process. International Journal of Greenhouse Gas Control 112, 103430. https://doi.org/10.1016/j.ijggc.2021.103430.

Greco-Coppi, M., Hofmann, C., Walter, D., Ströhle, J., Epple, B., 2023. Negative CO_2 emissions in the lime production using an indirectly heated carbonate looping process. Mitig Adapt Strateg Glob Change 28. https://doi.org/10.1007/s11027-023-10064-7.

Haaf, M., Anantharaman, R., Roussanaly, S., Ströhle, J., Epple, B., 2020a. CO_2 capture from waste-to-energy plants: Techno-economic assessment of novel integration concepts of calcium looping technology. Resources, Conservation and Recycling 162, 104973. https://doi.org/10.1016/j.resconrec.2020.104973.

Haaf, M., Hilz, J., Peters, J., Unger, A., Ströhle, J., Epple, B., 2020b. Operation of a 1 MW_{th} calcium looping pilot plant firing waste-derived fuels in the calciner. Powder Technology 372, 267–274. https://doi.org/10.1016/j.powtec.2020.05.074.

Haaf, M., Müller, A., Unger, A., Ströhle, J., Epple, B., 2020c. Combustion of solid recovered fuels in a semi-industrial circulating fluidized bed pilot plant - Implications of bed material and combustion atmosphere on gaseous emissions. VGB Power Tech 3, 51–56.

Haaf, M., Peters, J., Hilz, J., Unger, A., Ströhle, J., Epple, B., 2020d. Combustion of solid recovered fuels within the calcium looping process – Experimental demonstration at 1 MW_{th}

scale. Experimental Thermal and Fluid Science 113, 110023. https://doi.org/10.1016/j.expthermflusci.2019.110023.
Haider, F., Horn, S., Waldmann, B., Warnecke, R., 2008. Quantifizierung des Korrosionsdiagramms auf der Basdis von Messungen mit der Augsburger Korrosionssonde. VDI-Korrosions-Tagung, 2008.06.12-13 in Oberhausen.
Hanak, D.P., Biliyok, C., Yeung, H., Białecki, R., 2014. Heat integration and exergy analysis for a supercritical high-ash coal-fired power plant integrated with a post-combustion carbon capture process. Fuel 134, 126–139. https://doi.org/10.1016/j.fuel.2014.05.036.
Hawthorne, C., Trossmann, M., Galindo Cifre, P., Schuster, A., Scheffknecht, G., 2009. Simulation of the carbonate looping power cycle. Energy Procedia 1, 1387–1394. https://doi.org/10.1016/j.egypro.2009.01.182.
Hills, T.P., 2016. Investigations of the use of spent sorbent from the Ca looping process in cement manufacture and investigation of long-term CO2 uptake in cement and concrete. PhD Thesis. Imperial College London.
Hills, T.P., Sceats, M., Rennie, D., Fennell, P., 2017. LEILAC: Low Cost CO_2 Capture for the Cement and Lime Industries. Energy Procedia 114, 6166–6170. https://doi.org/10.1016/j.egypro.2017.03.1753.
Hoeftberger, D., Karl, J., 2016. The Indirectly Heated Carbonate Looping Process for CO_2 Capture—A Concept With Heat Pipe Heat Exchanger. Journal of Energy Resources Technology 138, 042211, 148A. https://doi.org/10.1115/1.4033302.
Hofmann, C., Greco-Coppi, M., Ströhle, J., Epple, B., 2022a. Operation of a 300 kW_{th} Indirectly Heated Carbonate Looping Pilot Plant for CO_2 Capture from Lime Industry. Fluidized Bed Conversion Conference, 8-11th May 2022, Chalmers University of Technology (Sweden).
Hofmann, C., Greco-Coppi, M., Ströhle, J., Epple, B., 2022b. Pilot Testing of the Indirectly Heated Carbonate Looping Process for Cement and Lime Plants. Proceedings of the 16th Greenhouse Gas Control Technologies Conference (GHGT-16) 23-24 Oct 2022. https://doi.org/10.2139/ssrn.4278810.
Hofmann, C., Greco-Coppi, M., Ströhle, J., Epple, B., 2024. Enhancement of a 300 kWth pilot plant for testing the indirectly heated carbonate looping process for CO2 capture from lime and cement industry. Experimental Thermal and Fluid Science 151, 111091. https://doi.org/10.1016/j.expthermflusci.2023.111091.
Hong, W.Y., 2022. A techno-economic review on carbon capture, utilisation and storage systems for achieving a net-zero CO2 emissions future. Carbon Capture Science & Technology 3, 100044. https://doi.org/10.1016/j.ccst.2022.100044.
Huang, Y., Keatley, P., Chen, H.S., Zhang, X.J., Rolfe, A., Hewitt, N.J., 2018. Techno-economic study of compressed air energy storage systems for the grid integration of wind power. Int. J. Energy Res. 42, 559–569. https://doi.org/10.1002/er.3840.
IEA, 2020. Energy Technology Perspectives 2020 - Special Report on Carbon Capture Utilisation and Storage: CCUS in clean energy transitions. OECD; OECD Publishing, Paris, 174 pp.
Junk, M., Reitz, M., Ströhle, J., Epple, B., 2013. Thermodynamic Evaluation and Cold Flow Model Testing of an Indirectly Heated Carbonate Looping Process. Chem. Eng. Technol. 36, 1479–1487. https://doi.org/10.1002/ceat.201300019.
Junk, M., Reitz, M., Ströhle, J., Epple, B., 2016. Technical and Economical Assessment of the Indirectly Heated Carbonate Looping Process. Journal of Energy Resources Technology 138, 042210. https://doi.org/10.1115/1.4033142.

Kemper, J., 2015. Biomass and carbon dioxide capture and storage: A review. International Journal of Greenhouse Gas Control 40, 401–430. https://doi.org/10.1016/j.ijggc.2015.06.012.

Kremer, J., Galloy, A., Ströhle, J., Epple, B., 2013. Continuous CO_2 Capture in a 1-MW_{th} Carbonate Looping Pilot Plant. Chem. Eng. Technol. 36, 1518–1524. https://doi.org/10.1002/ceat.201300084.

Krishnan, A., Nighojkar, A., Kandasubramanian, B., 2023. Emerging towards zero carbon footprint via carbon dioxide capturing and sequestration. Carbon Capture Science & Technology 9, 100137. https://doi.org/10.1016/j.ccst.2023.100137.

Kunii, D., Levenspiel, O., 1991. Fluidization Engineering, 2nd ed., 508 pp.

Lasheras, A., Ströhle, J., Galloy, A., Epple, B., 2011. Carbonate looping process simulation using a 1D fluidized bed model for the carbonator. International Journal of Greenhouse Gas Control 5, 686–693. https://doi.org/10.1016/j.ijggc.2011.01.005.

Madejski, P., Chmiel, K., Subramanian, N., Kuś, T., 2022. Methods and Techniques for CO_2 Capture: Review of Potential Solutions and Applications in Modern Energy Technologies. Energies 15, 887. https://doi.org/10.3390/en15030887.

Martínez, I., Murillo, R., Grasa, G., Rodríguez, N., Abanades, J.C., 2011. Conceptual design of a three fluidised beds combustion system capturing CO_2 with CaO. International Journal of Greenhouse Gas Control 5, 498–504. https://doi.org/10.1016/j.ijggc.2010.04.017.

Menny, K., 2006. Strömungsmaschinen: Hydraulische und thermische Kraft- und Arbeitsmaschinen ; mit 36 Tabellen und 47 Beispielen ; [mit h,s-(Mollier)-Diagramm, 5th ed. Teubner, Wiesbaden, 327 pp.

Mignard, D., 2014. Correlating the chemical engineering plant cost index with macro-economic indicators. Chemical Engineering Research and Design 92, 285–294. https://doi.org/10.1016/j.cherd.2013.07.022.

Moora, H., Roos, I., Kask, U., Kask, L., Ounapuu, K., 2017. Determination of biomass content in combusted municipal waste and associated CO_2 emissions in Estonia. Energy Procedia 128, 222–229. https://doi.org/10.1016/j.egypro.2017.09.059.

Myöhänen, K., Hyppänen, T., Pikkarainen, T., Eriksson, T., Hotta, A., 2009. Near Zero CO_2 Emissions in Coal Firing with Oxy-Fuel Circulating Fluidized Bed Boiler. Chem. Eng. Technol. 32, 355–363. https://doi.org/10.1002/ceat.200800566.

Qu, Z., Zhong, R., Wang, L., Zhao, W., Tian, X., Wang, H., 2020. Research Progress on High Temperature Corrosion Mechanism of Waste Incineration Power Generation Boiler. IOP Conf. Ser.: Earth Environ. Sci. 598, 12008. https://doi.org/10.1088/1755-1315/598/1/012008.

Ramkumar, S., Fan, L.-S., 2010. Thermodynamic and Experimental Analyses of the Three-Stage Calcium Looping Process. Ind. Eng. Chem. Res. 49, 7563–7573. https://doi.org/10.1021/ie100846u.

Reeves, E., Smith, C., Johnson, A., Stalbow, N., Antypas, I., Nierinck, J., 2023. Energy from Waste to be included in the EU Emissions Trading System. https://www.ashurst.com/en/insights/energy-from-waste-to-be-included-in-the-eu-emissions-trading-system/ (accessed 9 June 2023).

Reitz, M., Junk, M., Ströhle, J., Epple, B., 2014. Design and Erection of a 300 kW_{th} Indirectly Heated Carbonate Looping Test Facility. Energy Procedia 63, 2170–2177. https://doi.org/10.1016/j.egypro.2014.11.236.

Reitz, M., Junk, M., Ströhle, J., Epple, B., 2016. Design and operation of a 300 kW_{th} indirectly heated carbonate looping pilot plant. International Journal of Greenhouse Gas Control 54, 272–281. https://doi.org/10.1016/j.ijggc.2016.09.016.

Rolfe, A., Huang, Y., Haaf, M., Pita, A., Rezvani, S., Dave, A., Hewitt, N.J., 2018a. Technical and environmental study of calcium carbonate looping versus oxy-fuel options for low CO_2 emission cement plants. International Journal of Greenhouse Gas Control 75, 85–97. https://doi.org/10.1016/j.ijggc.2018.05.020.

Rolfe, A., Huang, Y., Haaf, M., Rezvani, S., MclIveen-Wright, D., Hewitt, N.J., 2018b. Integration of the calcium carbonate looping process into an existing pulverized coal-fired power plant for CO2 capture: Techno-economic and environmental evaluation. Applied Energy 222, 169–179. https://doi.org/10.1016/j.apenergy.2018.03.160.

Romano, M.C., Spinelli, M., Campanari, S., Consonni, S., Cinti, G., Marchi, M., Borgarello, E., 2013. The Calcium Looping Process for Low CO2 Emission Cement and Power. Energy Procedia 37, 7091–7099. https://doi.org/10.1016/j.egypro.2013.06.645.

Roussanaly, S., 2019. Calculating CO_2 avoidance costs of Carbon Capture and Storage from industry. Carbon Management 10, 105–112. https://doi.org/10.1080/17583004.2018.1553435.

Roussanaly, S., Fu, C., Voldsund, M., Anantharaman, R., Spinelli, M., Romano, M., 2017. Techno-economic Analysis of MEA CO_2 Capture from a Cement Kiln – Impact of Steam Supply Scenario. Energy Procedia 114, 6229–6239. https://doi.org/10.1016/j.egypro.2017.03.1761.

Santos, M.P.S., Hanak, D.P., 2022. Carbon capture for decarbonisation of energy-intensive industries: a comparative review of techno-economic feasibility of solid looping cycles. Front. Chem. Sci. Eng. 16, 1291–1317. https://doi.org/10.1007/s11705-022-2151-5.

Sarc, R., Lorber, K.E., 2013. Production, quality and quality assurance of Refuse Derived Fuels (RDFs). Waste management (New York, N.Y.) 33, 1825–1834. https://doi.org/10.1016/j.wasman.2013.05.004.

Schorcht, F., Kourti, I., Scalet, B.M., Roudier, S., Delgado Sancho, L., 2013. Best available techniques (BAT) reference document for the production of cement, lime and magnesium oxide: Industrial Emissions Directive 2010/75/EU (integrated pollution prevention and control). Publications Office, Luxembourg, 475 pp.

Shimizu, T., Hirama, T., Hosoda, H., Kitano, K., Inagaki, M., Tejima, K., 1999. A Twin Fluid-Bed Reactor for Removal of CO_2 from Combustion Processes. Chemical Engineering Research and Design 77, 62–68. https://doi.org/10.1205/026387699525882.

Simbeck, D., Beecy, D., 2011. The CCS paradox: The much higher CO_2 avoidance costs of existing versus new fossil fuel power plants. Energy Procedia 4, 1917–1924. https://doi.org/10.1016/j.egypro.2011.02.071.

Steag Energy Services GmbH, 2022. EBSILON®*Professional* Version 16.0.0.32608 [Computer software]. https://www.ebsilon.com/de/.

Ströhle, J., Hofmann, C., Greco-Coppi, M., Epple, B., 2021. CO_2 Capture From Lime and Cement Plants Using an Indirectly Heated Carbonate Looping Process - The ANICA Project, in: TCCS-11: CO_2 capture, transport and storage, Trondheim, 22nd-23rd June 2021: Short papers from the 11th International Trondheim CCS Conference, Trondheim, Norway. June 21-23. SINTEF Academic Press, Oslo, pp. 529–535.

Ströhle, J., Junk, M., Kremer, J., Galloy, A., Epple, B., 2014. Carbonate looping experiments in a 1MW_{th} pilot plant and model validation. Fuel 127, 13–22. https://doi.org/10.1016/j.fuel.2013.12.043.

Telesca, A., Calabrese, D., Marroccoli, M., Tomasulo, M., Valenti, G.L., Duelli, G., Montagnaro, F., 2014. Spent limestone sorbent from calcium looping cycle as a raw material for the cement industry. Fuel 118, 202–205. https://doi.org/10.1016/j.fuel.2013.10.060.

Telesca, A., Marroccoli, M., Tomasulo, M., Valenti, G.L., Dieter, H., Montagnaro, F., 2015. Calcium looping spent sorbent as a limestone replacement in the manufacture of portland and calcium sulfoaluminate cements. Environmental science & technology 49, 6865–6871. https://doi.org/10.1021/acs.est.5b00394.

Tilak, P., El-Halwagi, M.M., 2018. Process integration of Calcium Looping with industrial plants for monetizing CO_2 into value-added products. Carbon Resources Conversion 1, 191–199. https://doi.org/10.1016/j.crcon.2018.07.004.

UK Government Digital Service, 2023. Landfill Tax increase in rates. Policy paper. https://www.gov.uk/government/publications/landfill-tax-rates-for-2023-to-2024/landfill-tax-increase-in-rates (accessed 5 November 2023).

Ulster University, 1992. ECLIPSE process simulator. Energy Research Centre, University of Ulster, Coleraine, Copyright 1992 [Computer software].

Velis, C.A., Longhurst, P.J., Drew, G.H., Smith, R., Pollard, S.J.T., 2010. Production and Quality Assurance of Solid Recovered Fuels Using Mechanical—Biological Treatment (MBT) of Waste: A Comprehensive Assessment. Critical Reviews in Environmental Science and Technology 40, 979–1105. https://doi.org/10.1080/10643380802586980.

Vitillo, J.G., Smit, B., Gagliardi, L., 2017. Introduction: Carbon Capture and Separation. Chemical reviews 117, 9521–9523. https://doi.org/10.1021/acs.chemrev.7b00403.

Voldsund, M., Gardarsdottir, S., Lena, E. de, Pérez-Calvo, J.-F., Jamali, A., Berstad, D., Fu, C., Romano, M., Roussanaly, S., Anantharaman, R., Hoppe, H., Sutter, D., Mazzotti, M., Gazzani, M., Cinti, G., Jordal, K., 2019. Comparison of Technologies for CO_2 Capture from Cement Production—Part 1: Technical Evaluation. Energies 12, 559. https://doi.org/10.3390/en12030559.

Wang, W., Ramkumar, S., Li, S., Wong, D., Iyer, M., Sakadjian, B.B., Statnick, R.M., Fan, L.-S., 2010. Subpilot Demonstration of the Carbonation−Calcination Reaction (CCR) Process: High-Temperature CO_2 and Sulfur Capture from Coal-Fired Power Plants. Ind. Eng. Chem. Res. 49, 5094–5101. https://doi.org/10.1021/ie901509k.

Wang, Y., Lin, S., Suzuki, Y., 2007. Study of Limestone Calcination with CO_2 Capture: Decomposition Behavior in a CO_2 Atmosphere. Energy Fuels 21, 3317–3321. https://doi.org/10.1021/ef700318c.

Wang, Y.D., Huang, Y., McIlveen-Wright, D., McMullan, J., Hewitt, N., Eames, P., Rezvani, S., 2006. A techno-economic analysis of the application of continuous staged-combustion and flameless oxidation to the combustor design in gas turbines. Fuel Processing Technology 87, 727–736. https://doi.org/10.1016/j.fuproc.2006.02.003.

Warnecke, R., 2004. Einfluss von Strömung und chemischen Reaktionen im rauchgasseitigen Belag auf Korrosion an Überhitzer-Rohern in Müllverbrennungsanlagen. VGB PowerTech 9/2004, 52–59.

Williams, B.C., McMullan, J.T., 1996. Techno-economic analysis of fuel conversion and power generation systems — the development of a portable chemical process simulator with capital cost and economic performance analysis capabilities. Int. J. Energy Res. 20, 125–142. https://doi.org/10.1002/(SICI)1099-114X(199602)20:2%3C125:AID-ER239%3E3.0.CO;2-2.

Yang, F., Meerman, J.C., Faaij, A., 2021. Carbon capture and biomass in industry: A techno-economic analysis and comparison of negative emission options. Renewable and Sustainable Energy Reviews 144, 111028. https://doi.org/10.1016/j.rser.2021.111028.

Zhao, M., Minett, A.I., Harris, A.T., 2013. A review of techno-economic models for the retrofitting of conventional pulverised-coal power plants for post-combustion capture (PCC) of CO_2. Energy Environ. Sci. 6, 25–40. https://doi.org/10.1039/C2EE22890D.

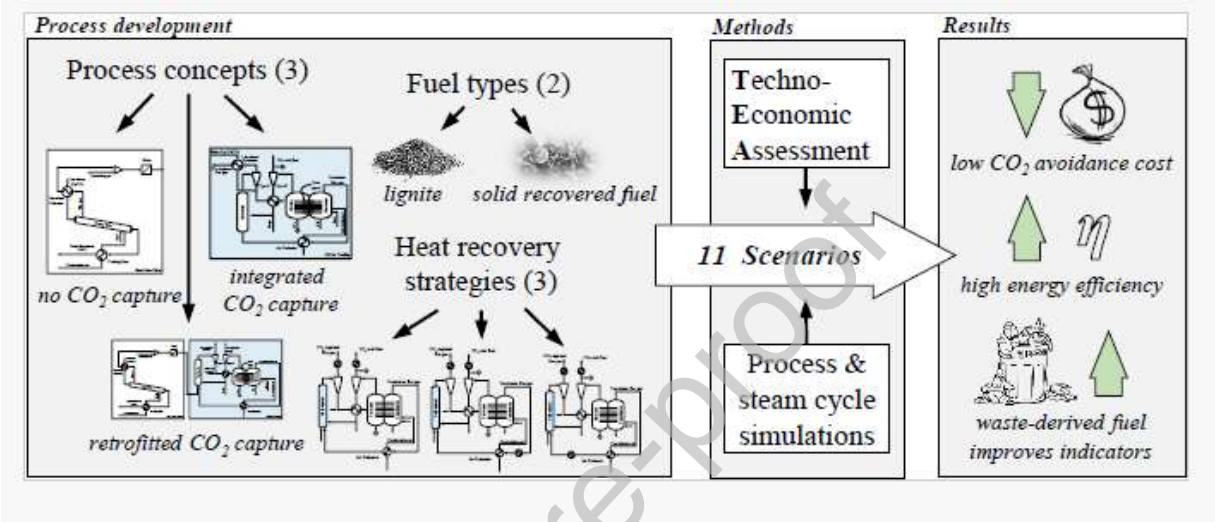

Declaration of interests

☐The authors declare that they have no known competing financial interests or personal relationships that could have appeared to influence the work reported in this paper.

☒The authors declare the following financial interests/personal relationships which may be considered as potential competing interests:

Martin Greco Coppi reports financial support was provided by German Federal Ministry for Economic Affairs and Climate Action. Angela Rolfe reports financial support was provided by Department for Business, Energy and Industrial Strategy of the United Kingdom. Martin Greco Coppi, Carina Hofmann, Jochen Ströhle, and Bernd Epple have patent #10 2023 114 353.9, "Apparatus and Method for Producing Lime" (German Patent and Trademark Office) pending to Technical University of Darmstadt.